August 18, 2003

DEVELOPMENT OF SELF CONSISTENT REGIONAL SOIL ATTENUATION RELATIONS FOR GROUND MOTIONS AND LIQUEFACTION PARAMETERS; AN EXAMPLE FOR THE BASIN AND RANGE REGION

Walter Silva*, Nick Gregor*, Robert Darragh*

Background

One of the Most Damaging Aspects of earthquakes is liquefaction-induced ground failure. Under strong ground shaking, pore water pressure builds up in saturated unconsolidated soils. If the induced shear-strains are large enough over a long enough duration, the pore water pressure can equal or exceed the overburden pressure resulting in a loss of shear strength or soil failure (Seed and Idriss, 1971; Silver and Seed, 1971). On level ground, lifelines may fail and buildings sink or topple due to differential settlements and massive land slides can be induced on sloping ground. Recent earthquakes such as the M 7.6 Chi-Chi, Taiwan; M 7.5 Koaceli, Turkey; M 6.9 Kobe, Japan; M 6.7 Northridge; and M 6.9 Loma Prieta have resulted in hundreds of billions of dollars in damage and years of reconstruction with much of the loss attributed to liquefaction related effects. Relic liquefaction of past earthquakes have reveled massive zones of soil failure suggesting a reoccurrence of the 1812 New Madrid and 1886 Charleston earthquakes could result in catastrophic damage to the infrastructure and potential loss of life (Obermeier et al., 1984, 1985, 1986).

While the basic engineering approaches to evaluating liquefaction susceptibility are well established and validated, methods of estimating onset of liquefaction that properly incorporate uncertainties in earthquake source, path, and site processes are needed to better assess risk levels and mitigate loss of life and property. An approach that rigorously captures uncertainties in assessing a soil's resistance to liquefaction in terns of cyclic demands is an essential step in better quantifying earthquake hazard and resulting risk to life and property.

Ground shaking and fault displacement from large earthquakes also cause heavy damage when they occur in or near metropolitan areas, but the uncertainties associated with their predictions are reasonably well characterized, particularly in tectonically active regions. There are many hundreds of recordings of ground shaking covering rupture distances of 1 to 200 km, varying site conditions from rock to soft soil and, for crustal sources, magnitudes ranging from about 4.5 to 7.5. Additionally, there has been no shortage of theoretical models developed and validated with varying degrees of sophistication in source, path, and site processes. These studies have produced predictive relations for both tectonically active and cratonic regions as well as subduction zones, quantifying strong ground shaking and its uncertainty and how they relate to magnitude, distance, and site condition. Because these ground motion relations characterize not only expected

* *Pacific Engineering and Analysis, 311 Pomona Ave., El Cerrito, CA 94530
www.pacificengineering.org; e-mail: pacificengineering@juno.com

values of response spectral ordinates but their uncertainties as well, decisions regarding levels of risk to structures and lifelines are possible. Additionally fully probabilistic ground shaking hazard assessments, now the standard of practice, can reliably estimate any fractile of expected ground shaking, fully accommodating uncertainties in earthquake sources (locations, magnitudes, and likelihoods of occurrence) as well as ground motions or shaking levels, conditional on **M**, *D*, and site condition (Abrahamson and Shedlock, 1997).

While noteable efforts have been made to characterize the probability of liquefaction (Halder and Tang, 1979; McGuire et al., 1979; Elton and Hamou, 1990; Power et al., 1991), conditional on soil column susceptibility (Liao et al., 1988) and magnitude (Loertscher and Youd, 1994; Youd and Idriss, 1997; Seed et al., 2001), the effects of uncertainties in source, path, and site processes on the onset of liquefaction have largely been ignored (Yegian and Whitman, 1978; Atkinson et al., 1984; Kavazanjian et al., 1985; Rockaway et al., 1997). The current state of practice in assessing the onset of liquefaction is fundamentally deterministic (National Research Council, 1985; Glaser and Chung, 1995; Yound and Idriss, 1997) and relies on estimates of expected peak accelerations (generally median values), soil properties (SPT, CPT, shear-wave velocity, Andrus et al., 1999), and empirical comparisons to case history data (CRR). Generally no formal accommodation for uncertainties in the ground shaking, soil material properties, or empirical observations of case histories are accommodated in estimates of the onset of liquefaction. As a result, the methodology, by design, is conservative (Silva and Costantino, 1999) with the degree of conservatism largely unquantified. A first step in formally accounting for uncertainty in the prediction of liquefaction resistance is to incorporate source, path, and site process parametric uncertainty into estimates of the seismic demands as well as capacities (CRR). This will allow more informed and rational decisions regarding risk levels to be made, an essential element in reducing losses due to earthquakes.

Current Methods of Evaluating Liquefaction Potential

The current state of practice in predicting liquefaction resistance of soils in the United States and much of the world is the method pioneered by H. Seed (Seed and Idriss, 1971; Martin et al., 1975; Youd and Idriss, 1997). In this approach, termed the simplified procedure, blow count from the Standard Penetration Test (SPT) is correlated with a parameter representing the seismic demands on the soil. The demands are expressed as the ratio of the average seismic induce shear-stress to the total vertical effective stress within a liquefiable zone, generally within about 50 ft of the surface,

$$CSR = \frac{\tau_{xy}}{\sigma_v^1} \qquad \text{(Seed and Idriss, 1971)} \qquad (1).$$

In practice, demands are usually computed using approximate relations between surface peak acceleration and at-depth cyclic shear stress (Seed and Idriss, 1971; Seed et al., 1983; Youd and Idriss, 1997; Seed et al., 2001).

Analyses of case histories for sites that had liquefied and those that did not, but could have, results in a reasonably good separation between the liquefied and non-liquefied

sites, with a deterministic boundary defined as the soils capacity to resist liquefaction or cyclic resistance ratio (CRR) (Youd and Idriss, 1997). Demands (CSR) that exceed the capacity (CRR) result in a factor of safety (CRR/CSR) less than 1 and liquefaction may be expected to occur. The capacity for a given soil deposit is either empirical (case histories, Figure 1) or determined from stress controlled laboratory testing procedures. Both capacities and demands depend upon soil properties such as relative density, fines content (particle size), clay content, geologic age and water content (depth of water table), degree of over consolidation, cementation, previous liquefaction history as well as amplitude and duration of earthquake excitation.

Subsequent to the introduction of the simplified procedure in 1971, the approach has been updated and revised a number of times (Seed, 1979; Seed and Idriss, 1982; Seed et al., 1983; Youd and Idriss, 1997). Correlations based on the Cone Penetration Test (CPT), the Becher Penetration Test (BPT), as well as shear-wave velocity have been developed over the interveaning years (Youd and Idriss, 1997; Andrus et al., 1999; Andrus and Stokoe, 2000).

As an alternative to shear stress, shear strain has been shown to be the fundamental controlling factor controlling the buildup of pore water pressure during cyclic loading (Dobry et al., 1981; 1982). An alternative strain based procedure for assessing the liquefaction potential of a soil was developed by Dobry et al. (1982) where

$$Es = \int \tau_{xy}\, d\gamma_{xy} \qquad (2)$$

is the strain energy (generally expressed in PSI) and τ_{xy} and γ_{xy} are the induced cyclic shear-stresses and strains respectively. As in the stress based approach, the strain energy density is evaluated over the depth of the liquefiable zone. This approach, although fundamentally sound, has not been widely applied among the geotechnical community.

More recently, an approach based on the energy content of ground shaking through Arias Intensity has been proposed as a measure of seismic demand (Davis and Berrill, 1978; Kayen and Mitchell, 1997). Rather than using either the stress or strain based approaches (Equation 1 or 2), Kayen and Mitchell (1997) correlated liquefaction resistance with the total horizontal component Arias intensity

$$I_h = I_{xx} + I_{yy} = \frac{\pi}{2g}\left[\int a_x^2(t)\, dt + \int a_y^2(t)\, dt\right] \qquad (3)$$

averaged over the liquefiable zone (depth range) in the soil column. The usual units used are m/sec (or cm/sec) and the integral expressions are a direct measure of the energy input to the soil column. As with the stress and strain based approaches, analyses of empirical case histories showed that liquefied and non-liquefied sites separate out, similar to Figure 1 with I_h replacing CSR defining an equivalent Intensity resistance ratio and a means of assessing the onset of liquefaction based on capacity (resistance to liquefaction) and demand (energy input to the soil column).

The ground motion energy approach is intuitively appealing as one expects that energy is a fundamental measure of demands or loads placed on a soil column. However, energy is

also fundamentally a nonlinear parameter and how soil columns with varying dynamic material properties convert the energy into actual work in increasing pore pressure and rearranging particles is poorly understood and may lead to large uncertainties in predicting demands. As with the strain energy density, the use of ground motion energy parameterized through total Arias Intensity shows promise but has not enjoyed widespread use in the geotechnical engineering practice.

Uncertainties in Estimating Liquefaction Resistance

The liquefaction resistance of soils is related to numerous geological, compositional, and state factors (Kramer, 1996). Geological factors include the age of the soil deposit, depositional environment, and hydrological conditions. In general, Holocene-age deposits are more prone to liquefaction than Pleistocene-age soils. Liquefaction occurs in saturated, cohesionless soils and thus depth to the groundwater table is an important consideration in identifying soils that are susceptible to liquefaction. Compositional factors that influence liquefaction resistance include grain size parameters such as the fines content and fabric-related parameters such as cementation. Finally, state factors such as the density, current state of stress, and stress history also have an important influence on liquefaction resistance. To the extent that these soil properties vary spatially, the liquefaction resistance will also vary.

Accommodating Uncertainties In Estimating Cyclic Demands

The stress, strain, and energy approaches to predicting the onset of liquefaction all share common features in estimating seismic demands: both dynamic material properties as well as the character of the seismic loads (stress time histories) are controlling factors. As a result, uncertainty and randomness (epistemic and aleatory variability, Roblee et al., 1996) in dynamic material properties as well as control motions should be accommodated in estimating cyclic demands. An approach that properly accommodates variability will not only result in fractiles for deterministic estimates demands, from which more informed risk decisions can be made, but provide a more rational basis for fully probabilistic assessments of liquefaction potential. Additionally the incorporation of parametric variability allows statistically rigorous assessments to be made of which parameters or suites of parameters control the cyclic demands. With this information, one can rationally design site sampling and testing programs to achieve desired degrees of accuracy as well as ascertain obtainable levels of accuracy, given the variability in control motions. Additionally one can easily evaluate the robustness or sensitivity to input parameters of the three currently available approaches to computing demands. This aspect alone may be significant as a lack of robustness in demand estimates must be compensated by increased accuracy in estimating capacity, since the factor of safety, or estimator of liquefaction likelihood, is the ratio of capacity to demand.

Equivalent-Linear Site Response Analyses

Each of the approaches to estimating the onset of liquefaction require site response analyses, either on a case by case basis or in developing simplified procedures, which assume generic material properties (Seed and Idriss, 1971; Kayen and Mitchell, 1997; Youd and Idriss, 1997; Seed et al., 2001). Given the seismic loads (control motions or motions input at the base of the soil column), the site response analyses accommodate

vertically varying dynamic material properties as well as material nonlinearities. Generally vertically propagating shear-waves are assumed and nonlinear site response is approximated through the equivalent-linear approach.

The equivalent-linear approach, in its present form, was introduced by Seed and Idriss (1970). This scheme is a particular application of the general equivalent-linear theory developed by Iwan (1967). Basically, the approach is to approximate a second order nonlinear equation, over a limited range of its variables, by a linear equation. Formally this is done in such a way that the average of the difference between the two systems is minimized. This was done in an ad-hoc manner for ground response modeling by defining an effective strain which is assumed to exist for the duration of the excitation. This value is usually taken as 65% (although other values have been used) of the peak time-domain strain calculated at the midpoint of each layer, using a linear analysis. Modulus reduction and hysteretic damping curves are then used to define new parameters for each layer based on the effective strain computations. The linear response calculation is repeated, new effective strains evaluated, and iterations performed until the changes in parameters are below some tolerance level. Generally a few iterations are sufficient to achieve a strain-compatible linear solution. This stepwise analysis procedure was formalized into a one-dimensional, vertically propagating shear-wave code called SHAKE (Schnabel et al., 1972). Subsequently, this code has easily become the most widely used analysis package for one-dimensional site response calculations.

The advantages of the equivalent-linear approach are that parameterization of complex nonlinear soil models is avoided and the mathematical simplicity of a linear analysis is preserved. A truly nonlinear approach requires the specification of the shapes of hysteresis curves and their cyclic dependencies through an increased number of material parameters. In the equivalent-linear methodology the soil data are utilized directly and, because at each iteration the problem is linear and the material properties are frequency independent, the damping is rate independent and hysteresis loops close.

Careful validation exercises between equivalent-linear and fully nonlinear formulations using recorded motions from 0.05 to 0.50g showed little difference in results (EPRI, 1993). Both formulations compared very favorably to recorded motions suggesting both the adequacy of the vertically propagating shear-wave model and the approximate equivalent-linear formulation. While the assumptions of vertically propagating shear-waves and equivalent-linear soil response certainly represent approximations to actual conditions, their combination has achieved demonstrated success in modeling observations of site effects and represent a stable, mature, and reliable means of estimating the effects of site conditions on strong ground motions (Schnabel et al., 1972; Silva et al., 1988; Schneider et al., 1993; EPRI, 1993; Silva et al., 1997).

To accommodate both uncertainty and randomness in dynamic material properties, SHAKE analyses are typically done for the best estimate shear-wave velocity profile as well as upper- and lower-range profiles. The upper- and lower-ranges are usually specified as twice and one-half the best estimate shear-wave moduli. Depending upon the nature of the structure, the final design spectrum or cyclic demands are then based upon an envelope or average of the analyses.

RVT Based Computational Scheme

The computational scheme employed to compute the site response for this proposed work uses an alternative approach employing random vibration theory (RVT). In this approach the control motion power spectrum is propagated through the one-dimensional soil profile using the plane-wave propagators of Silva (1976). In this formulation only SH waves are considered. Arbitrary angles of incidence may be specified but normal incidence is generally used.

In order to treat possible material nonlinearities, an RVT based equivalent-linear formulation is employed. Random process theory is used to predict peak time domain values of shear-strain based upon the shear-strain power spectrum. In this sense the procedure is analogous to the program SHAKE except that peak shear-strains in SHAKE are measured in the time domain. The purely frequency domain approach obviates a time domain control motion and, perhaps just as significant, eliminates the need for a suite of analyses based on different input motions. This arises because each time domain analysis may be viewed as one realization of a random process. Different control motion time histories reflecting different time domain characteristics but with nearly identical response spectra can result in different nonlinear and equivalent-linear response. In this case, several realizations of the random process must be sampled to have a statistically stable estimate of site response. The realizations are usually performed by employing different control motions with approximately the same level of peak accelerations and response spectra.

In the case of the frequency domain approach, the estimates of peak shear-strain as well as oscillator response are, as a result of the random process theory, fundamentally probabilistic in nature. For fixed material properties, stable estimates of site response can then be obtained with a single run and no time history is required.

Accommodating Parametric Uncertainty In Site Response Analyses

In the context of the RVT equivalent-linear approach, a more robust method of incorporating variability of dynamic material properties into the computed response has been developed. Because analyses with multiple time histories are not required, parametric variability can be accurately assessed through a Monte Carlo approach by randomly varying dynamic material properties. This results in median as well as other fractile levels (e.g. 16^{th}, mean, 84^{th}) of smooth response spectra at the surface of the site as well as liquefaction parameters with depth. The availability of fractile levels reflecting variability in dynamic material properties then permits a more rational basis for selecting levels of risk.

In order to randomly vary the shear-wave velocity profile, a profile randomization scheme has been developed which varies both layer velocity and thickness. The randomization is based on a correlation model developed from an analysis of variance on about 500 measured shear-wave velocity profiles (EPRI, 1993; Silva et al., 1997). Profile depth (depth to competent material) is also varied on a site specific basis using a uniform distribution. The depth range is generally selected to reflect expected variability over the area considered as well as uncertainty in the estimation of depth to competent material.

To accommodate variability in modulus reduction and hysteretic damping curves on a generic basis, the curves are independently randomized about base case values. A log normal distribution is assumed with a σ_{ln} of 0.30 at a cyclic shear strain of 3 x 10^{-2}%. These values are based on an analysis of variance of a suite of laboratory test results. An upper and lower bound truncation of 2σ is used to prevent modulus reduction or damping models that are not physically possible. The random curves are generated by sampling the transformed normal distribution with a σ_{ln} of 0.30, computing the change in normalized modulus reduction or percent damping at 3 x 10^{-2}% shear strain, and applying this factor at all strains. The random perturbation factor is reduced or tapered near the ends of the strain range to preserve the general shape of the base case curves (Silva, 1992; EPRI, 1993).

Accommodating Uncertainty In Control Motions

For model derived control motions, uncertainties in source and path parameters are accommodated by randomly varying their values following empirical distributions (EPRI, 1993; Toro et al., 1997). Both the point source (Boore 1983; 1986; Schneider et al., 1993) and finite-source stochastic models (Silva et al., 1990; Schneider et al., 1993; Atkinson and Silva, 1997, 2000; Schneider et al., 2000) have been combined with RVT equivalent-linear site response to enable randomly varying source, path, and site parameters in a convenient manner. Both combined models have recently been validated by modeling recorded motions at over 500 sites from 18 earthquakes (**M** 5 to 7.5) at rupture distances ranging from 1 to 480 km and for very stiff to very soft site conditions (Silva et al., 1997).

The point-source model forms the basis for the currently available attenuation relations for the central and eastern United States (Abrahamson and Shedlock, 1997; Toro and Silva, 2001; Toro et al., 1997; EPRI, 1993) and the finite-source model has been used to develop attenuation relations for subduction zone earthquakes (Youngs et al., 1997; Wong et al., 2000; Gregor et al., 2000) as well as scenario earthquake shaking maps for Portland (Wong et al., 2000), Salt Lake City (Wong et al., 2001a), Albuquerque (Wong et al., 2001b), and the San Francisco Bay Area (Schneider et al., 2000).

For the point-source model, source and path parameters that are generally varied include stress drop, Q(f), kappa (considered a path parameter when coupled to equivalent-linear site response), and source depth (EPRI, 1993; Toro et al., 1997). For the finite-source for large (**M** > 7) earthquakes, point-source stress drop and source depth are replaced by varying slip models as well as nucleation points (Silva, 1992; Roblee et al., 1996; Schneider et al., 2000; Atkinson and Silva, 1997, 2000). Source ruptures for a given scenario (**M**) are randomly initiated at hypocenters along the length of the fault, representing scenarios ranging from unilateral ruptures in opposite directions and various bilateral ruptures in between. The hypocenters are randomized within a nucleation zone (rectangle) which comprises the bottom half and to within 10% of the ends of the rupture surface. The sample distribution of hypocenters is used to model potential variations in source directivity. To represent other random effects of the rupture process, each scenario is generated from a suite of randomly selected slip distributions. The random slip models are generated using a simulation scheme that preserves asperity statistics such as size and number, given a rupture area. The statistics are based on slip models derived from modeling strong ground motions (Abrahamson et al., 1994). The combined

randomization of hypocenter locations and slip distributions results in a total of 30 source scenario combinations for the entire grid of site locations.

Model Parameters

For the point-source model implemented here, parameters include stress drop ($\Delta\sigma$), source depth (H), path damping ($Q(f) = Q_o f^{\eta}$), shallow crustal damping (kappa), and crustal amplification. The regional crust model from Pechmann (1999) was adopted. The crustal model is listed in Table 1. The Moho is at a depth of about 30 km. Geometrical attenuation of both ground motions is assumed to be magnitude dependent, using a model based on inversions of the Abrahamson and Silva (1997) empirical attenuation relation with the point-source model. The model for geometrical attenuation is given by

$$R^{-(a + b\,(\mathbf{M} - 6.5))}, \quad R \leq 80 \text{ km}; \qquad R^{-(a + b\,(\mathbf{M} - 6.5))/2}, \quad R > 70 \text{ km} \qquad (4)$$

where a = 1.0296, b = -0.0422, and 70 km reflects about twice the crustal thickness (Table 1).

The duration model is taken as the inverse corner frequency plus a smooth distance term of 0.05 times the hypocentral distance (Herrmann, 1985). Monotonic trends in both the geometrical attenuation and distance duration models produced no biases in the validation exercises using WNA and CENA recordings (Appendix A) and are considered appropriate when considerable variability in crustal structure that may exist over a region, as well as variability in source depth. Additionally, extensive modeling exercises have shown that the effects of source finiteness, coupled with variability in source depth and crustal structure, result in smooth attenuation with distance, accompanied by a large variability in ground motions (EPRI, 1993).

To model shallow crustal damping, a kappa value of 0.040 sec is assumed to apply for the crust (Silva and Darragh, 1995; EPRI, 1993). The Q(f) model is $Q(f) = 370\ f^{0.35}$. A magnitude dependent stress drop model is used. For this stress drop model, the stress drop varies from 60 bars for **M** 4.5 and 5.5 to 30 bars for **M** 7.5 and 70 bars for **M** 8.5 (the range in magnitudes for the simulations). The magnitude scaling of stress drop is based on point-source inversions of the Abrahamson and Silva (1997) empirical attenuation relation (Silva et al., 1997) and is an empirically driven mechanism to accommodate the observed magnitude saturation due to source finiteness. Similar point-source stress drop scaling has been observed by Atkinson and Silva (1997) using (WNA) recordings of strong ground motions and from inversions of the Sadigh et al., (1997) attenuation relation (EPRI, 1993). Recent observations of strong ground motion recordings from the BRNA region indicate lower average ground motions than those observed in active compressional/strike-slip regions for similar magnitude and distance values (Wong and Olig, 1998; Spudich et al., 1997; Stepp et al., 2001). The magnitude dependent stress drop values (see Table 2) used in this study have been adjusted to incorporate the empirical observation of reduced ground motions from extensional regions when compared to compressive tectonic regions.

Source depth is also assumed to be magnitude dependent and is based on the depth distribution of California Seismicity. The magnitude dependent depth distribution is shown in Table 2.

Because of the manner in which the model validations were performed ($\Delta\sigma$, Q(f), and H were optimized), parametric variability for only $\Delta\sigma$, Q(f) and H are required to be reflected in the model simulations (Appendix B; EPRI, 1993; Roblee et. al., 1996). For source depth variability, a lognormal distribution is used with a $\sigma_{ln} = 0.6$ (EPRI, 1993). Bounds are placed on the distribution to prevent nonphysical realizations (Table 2).

The stress drop variability, $\sigma_{ln} = 0.5$ is from Silva et al. (1997) and is based on inversions of ground motions for stress drop using California earthquakes. The variability in Q(f) is taken in Q_o alone ($\sigma_{ln} = 0.4$) and is based on inversions in WNA for Q(f) models. While not strictly required, the crust kappa (0.040 sec) was also varied since its value is based entirely on data from other WUS regions (Silva et al., 1997). The variability for kappa ($\sigma_{ln} = 0.3$) is based on the variability seen in kappa values determined from strong ground motions recorded at about 20 Northern California rock sites which recorded the **M** 6.9 1989 Loma Prieta earthquake (EPRI, 1993).

While this uncertainty of 0.3 for kappa may seem low to characterize both epistemic (uncertainty in the median value) and aleatory (uncertainty about the median value) variability in a site specific kappa value, the point-source modeling uncertainty (Appendix A; Silva et al., 1997) already accommodates the effects of kappa variability. This arises because a fixed kappa value of 0.03 sec was used to characterize the linear rock damping at all rock sites in the validation exercises. As a result, site-specific departures of kappa values from the assumed value of 0.03 sec increase model departures from recorded motions resulting in larger estimates of model uncertainty. While it is possible that the total variability in the attenuation relations has been overestimated due to this probable double counting, validations are sparse for the CENA (nonexistent for deep soil sites) and for **M** larger than about 7.0 in the WNA. As a result, assessment and partition of appropriate variability is not an unambiguous issue, particularly in the CENA, and the approach taken here is to follow prudent design practice and not underestimate uncertainty.

A generic deep soil profile was used in the analysis. This profile was developed based on a database of sheer wave profiles which were classified as being Geomatrix C and D sites (Silva et al., 1997). The profile variability was taken over the top 305m (1,000 feet), which is consistent with the deepest soil profile. This base case profile was randomized based on a correlation model developed from the observed profile database. Figure 1 is a plot of the base case soil profile.

Two sets of soil shear modulus reduction and damping curves were used in the analysis to accommodate epistemic variability in nonlinear dynamic material properties. The first set of material curves are from EPRI (1993) and are plotted in Figure 2a. This set of curves was developed through a suite of laboratory tests as well as an extensive literature search (EPRI 1993). They have been validated by modeling strong ground motions recorded in Northern California (Silva et al., 1997) and in Kobe, Japan (Silva, Costantino, and Iwasaki 1999). The second set of soil curves are from the Peninsula Range, California (Silva et al., 1997) and are plotted in Figure 2b. This set of curves is more linear than the EPRI curves and was developed by modeling strong ground motions recorded in the Los Angeles area as well as the soil motions in the Abrahamson and Silva

(1997) empirical attenuation relation (Silva et al., 1997). For these conditions the EPRI cohesionless soil curves resulted in a soil response which was too nonlinear. The two sets of curves are taken to reflect uncertainty in mean G/Gmax and hysteretic damping models. Below a depth of 152m (500 ft) the soil column was assumed to behave linearly, based on modeling of recorded strong ground motions recorded at deep soil sites (Silva et al., 1997).

Attenuation Relations For Earthquake Ground Motions

To generate data, which consists of 5% damped spectral acceleration, peak acceleration, peak particle velocity, and peak displacements, for the regression analyses, 30 simulations reflecting parametric variability are made at distances of 1, 5, 10, 20, 50, 75, 100, 200, and 400 km. At each distance, five magnitudes are used: **M** 4.5, 5.5, 6.5, 7.5, and 8.5 (Table 2).

The functional form selected for the regressions which provided the best overall fit (from a suite of about 25) to the simulations is given by

$$\ln y = C_1 + C_2\,\mathbf{M} + (C_6 + C_7\,\mathbf{M})^* \ln\left(R + e^{C4}\right) + C_{10}\,(\mathbf{M} - 6)^2, \quad (5)$$

where R is taken as a closest distance to the surface projection of the rupture surface, consistent with the validation exercises (Silva et al., 1997).

Figure 3 shows the simulations for peak accelerations as well as the model fits for **M** 7.5 for the EPRI material curves. In general, the model fits the central trends (medians) of the simulations. Figure 4 summarizes the magnitude dependency of the peak acceleration estimates (EPRI soil curves) and saturation is evident, due to the magnitude dependent stress drop and soil nonlinearity. Also evident is the magnitude dependent far-field fall off with a decrease in slope as **M** increases (easily seen beyond 100 km). The model predicts peak accelerations at a distance of 1 km of about 0.09, 0.20, 0.33, 0.48g for **M** 4.5, 5.5, 6.5, and 7.5, respectively.

An example of response spectra at 10 km for **M** 4.5, 5.5, 6.5, 7.5, and 8.5 are shown in Figure 5. For **M** 7.5, the peak acceleration (Sa at 100 Hz) is about 0.30g with the peak in the spectrum near 1.00 sec. The jagged nature of the spectra is due to unsmoothed coefficients. The model regression coefficients are listed (EPRI curves) in Table 3 along with the parametric and total variability. The modeling variability is taken from Appendix A. The total variability, solid line in Figure 6, ranges from about 1.5 at short periods to about 3.5 at a period of 5 sec where it is dominated by modeling variability. This large long period uncertainty is due to the tendency of the point-source model to overpredict low frequency motions at large magnitudes (**M** > 6.5; EPRI, 1993). This trend led Atkinson and Silva (1997, 2000) to introduce a double-corner point-source model for WUS crustal sources, suggesting a similarity in source processes for WUS and CEUS crustal sources, but with CEUS sources being more energetic by about a factor of two (twice WUS stress drops), on average.

Figure 7 gives the simulations for peak accelerations as well as the model fit for **M** 7.5

using the Peninsula Range soil curves. The magnitude dependence of the PGA model is shown in Figure 8. Peninsular Range G/Gmax and hysteretic damping cures (Figure 2a) compared to the EPRI curves (Figure 2b) result in higher short period motions, particularly at high loading levels. This is clearly reflected in the corresponding response spectra shown in Figure 9. The regression coefficients are listed in Table 3. Finally, the associated parametric, modeling, and total sigma is shown in Figure 10 motions computed using the Peninsula Range soil curves.

Attenuation Relations For Liquefaction Parameters

The evaluation of a soil's resistance to liquefaction involves the estimation of both the capacity to resist liquefaction as well as the demand placed on the soil by ground shaking (Youd and Idriss, 2001).

Site-specific evaluation of liquefaction resistance involves use of empirical correlations between the observed occurrence of liquefaction and the results of field measurements. Accepted field measurements include the standard penetration test (Seed and Idriss, 1971; Seed et al., 1976; Seed and Idriss, 1982; and Seed et al., 1983), the cone penetration test (Robertson and Campanella, 1985), and shear-wave velocity measurements (Andrus and Stokoe, 2000). All of these field measurements provide an indication of the soil's relative density. Relative density along with saturation conditions, effective stress, and grain size determine the soil's resistance to liquefaction, in terms of a cyclic resistance ratio (CRR).

For this study, the CRR for the soils was determined using the shear-wave velocity profiles and the estimated fines content (i.e., content of soil particles smaller than the 0.075 mm). A generic fine contents of 10% was used for this analysis. Use of the more widespread approach in estimating cyclic demands such as standard penetration and cone penetration tests would have involved developing median values of blow count and tip resistance as well as statistical models for the generic soil profile. The availability and maturity of statistical models for the variability of shear-wave velocities and layer thickness and nonlinear dynamic material properties were compelling arguments for implementing a shear-wave velocity approach to estimate cyclic capacities. It is recognized that other engineering approaches for determining the liquefaction resistance of soils may be considered more applicable on a site-specific basis. It may also be feasible to consider use of other field measurements, such as SPT or CPT data, for more refined analysis in areas of specific interest. In future studies, it may be desirable to evaluate the liquefaction resistance using correlations with either the SPT or CPT in areas where substantial data are available.

A particularly attractive advantage in using the shear-wave velocity approach in liquefaction assessment is that it is straightforward and it directly accommodates profile parametric uncertainty in estimates of CRR as well as CSR in a statistically rigorous manner. Shear-wave velocity, as well as nonlinear dynamic material properties, can be incorporated in a manner consistent with developing the ground motions, arriving at median and fractile estimates of liquefaction potential that are consistent with median and fractile estimates of ground motions. This is particularly important for loss estimation analyses (e.g., HAZUS) that are fundamentally based on both ground motions and

liquefaction (deformation), requiring the same fractile level for both hazards. The approach implemented in this study accomplishes this objective in a statistically rigorous manner.

The equation for determining the CRR from shear-wave velocity is empirical, and based on case history studies at sites that did and did not liquefy during earthquakes (Andrus and Stokoe, 2000). The equation is:

$$CRR = 0.022\,(K_C\,V^*_{S1}/100)^2 + 2.8\,[1/V^*_{S1} - K_C\,V_{S1})\text{-}1/V^*_{S1}] \cdot MSF \qquad (6)$$

$$MSF = (\mathbf{M}/7.5)^{-2.56} \qquad (7)$$

where V_{S1} is the stress-corrected shear-wave velocity, V^*_{S1} is the limiting upper value of V_{S1} for cyclic liquefaction occurrence that depends on fines content and K_C is a correction factor for cementation and aging. Because there is currently no widely accepted method for estimating K_C as well as its variability across the category areas (Andrus and Stokoe, 2000), it was taken as 1 for this study. A fines content value of 10% was used in this study.

Cyclic demands are expressed as the ratio of the average seismically-induced shear-stress to the vertical effective overburden stress within a liquefiable zone, generally within about 50 ft (15.2 m) of the ground surface:

$$CSR = \frac{\tau_{xy}}{\sigma'_v} \qquad \text{(Seed and Idriss, 1971)} \qquad (8)$$

In practice, demands are usually computed using approximate and generic relations between surface peak acceleration and at-depth cyclic shear stress (Seed and Idriss, 1971; Seed *et al.*, 1983; Youd and Idriss, 1997; Seed et al., 2001).

The ratio of capacity (CRR) to demand (CSR) is termed the factor of safety (FS) against liquefaction. Liquefaction is predicted to occur when FS is at or below 1, and not to occur when it exceeds 1. To provide a more rational basis for assessing risk levels, Juang *et al.* (2000, 2001) cast the deterministic factor of safety into an expression for the probability of liquefaction (P_L). This mapping function is given by:

$$P_L = 1/(1 + (FS/0.78)^{3.5}) \qquad (9)$$

It is based on the field performance data compiled by Andrus and Stokoe (2000) and accommodated the occurrence of sites that should have liquefied but did not, as well as those that did and provides the mechanism for translating liquefaction hazard into liquefaction risk. The Building Seismic Safety Council recommends a margin for the factor of safety against liquefaction of 1.2 to 1.5 for the simplified approach (Seed and Idriss, 1971). The corresponding probabilities are about 20% to 10% (Juang *et al.*, 2001). A factor of safety of 1 corresponds to a probability of about 30%.

For this study, the average CSR for the soil susceptible to liquefaction is determined during the site response analyses. Conditions which determine the CSR are: (1) cyclic

shear stresses induced by the earthquake throughout the liquefiable zone, (2) σ_{vo} – the total vertical overburden stress, and (3) σ'_{vo} – the effective vertical overburden stress. Calculation of the total and effective stress conditions requires estimation of the density of the overlying material. The following empirical correlation between shear-wave velocity and mass density (Mayne and Rix, 1993; Mayne and Rix; 1995; Hegazy and Mayne, 1995; and Burns and Mayne, 1996) was used to calculate the stress conditions:

$$\rho \text{ (mass density)} = 0.8 \log (V_s) \qquad (10)$$

The estimation of the liquefaction parameters was performed at each magnitude and distance values used in the ground motion dataset. The depth to the water table was placed at 3.048m (10 feet) and the average CSR, FS, and probability of liquefaction was computed over the depth range of 1.524m (5 feet) to 6.096m (20 feet).

The attenuation model used for the regression of the ground motion data (i.e., see equation (3)) was used in the regression analysis to develop the attenuation model for the 3 liquefaction parameters (i.e, CSR, FS, and PL). Figure 11 shows the CSR model for **M** 4.5 to 8.5 verses distance using the EPRI soil curves. As with the peak accelerations (Figure 4), the CSR values show magnitude saturation as well as the magnitude dependent far field slope. The parametric variability, $\sigma_{ln} = 0.4226$ (Table 3) is close to that of peak acceleration ($\sigma_{ln} = 0.4355$), reflecting the expected correspondence between the two (Seed and Idriss, 1971). The attenuation relation for CSR along with its variability can be used to provide deterministic estimates of fractile levels as well as used in probabilistic seismic hazard codes, all consistent with the ground motion hazard (Table 3). For the Factor of Safety, Figure 12 shows simulations and regression fit for **M** 7.5 while Figure 13 shows the model for **M** 4.5 to 8.5. As with the CSR regression model, magnitude saturation and the magnitude dependent for field increase are evident. The parametric variability ($\sigma_{ln} = 0.6825$) has increased by about 50% over that of the CSR ($\sigma_{ln} = 0.4226$) as the FS now includes the capacities and accompanying variability in shear-wave velocity (Equation 4). The parametric variability for the probability of liquefaction is unrealistically large, $\sigma_{ln} = 2.5134$ (Table 3), due to its extremely wide range, intrinsic to the logarithmic dependence (Equation 7). A factor of two change in the FS, from 1 to 2, results in a change in probability from about 30% to less than 4%, a factor of about 7. Clearly a more appropriate procedure is required for expressing the parametric variability associated with the probability of liquefaction. For **M** 7.5 the model would predict liquefaction (i.e. median FS values of 1 or less) for distance up to approximately 10 km. For **M** $\leq$ 6.5 earthquake, the attenuation model would not predict liquefaction to occur.

Finally, Figure 14 gives the probability of liquefaction model for the 5 magnitude values. Because the regression model for the probability of liquefaction was not constrained to be less than or equal to 1.0, unphysical results (i.e., probabilities of liquefaction of greater than 1.0) are predicted for larger magnitudes at close distances.

The similar sets of simulation and model results are plotted in Figures 15 to 18 for the Peninsula Range soil curves. These regression coefficients are listed in Table 4. The ground motion attenuation model from the Peninsula Range curves predicts larger short period ground motion values than the EPRI curves. These larger short period ground motion values lead to a lower FS model for the Peninsula Range curves. For a **M** 7.5 earthquake, the FS model shown in Figure 17 would predict liquefaction for distance less

than about 15 km. As was the case for the EPRI soil curve, no liquefaction is predicted for $\mathbf{M} \leq 6.5$ for distance greater than 1 km.

REFERENCES

Abrahamson, N.A. and W.J. Silva (1997). "Empirical response spectral attenuation relations for shallow crustal earthquakes." *Seismological Research Let.,* 68(1), 94-127.

Ackerman, H.D (1983). "Seismic refraction study in the area of the Charleston, South Carolina, 1886 earthquake, in studies related to the Charleston, South Carolina, earthquake of 1886 - tectonics and seismicity." G.S. Gohn, ed., *U.S. Geological Survey Professional Paper,* 1313-F, 20p.

Andrus, R.D., and Stokoe, K.H., II. (2000). "Liquefaction resistance of soils from shear-wave velocity," *Journal of Geotechnical and Geoenvironmental Engineering,* 126(11), 1015-1025.

Atkinson, G.M and W.J. Silva (2000). "A Stochastic modeling of California ground motions," *Bull. Seism. Soc. Am,.* 90(2), 255-274.

Atkinson, G.M. and D.M. Boore (1997). "Some comparisons between recent ground-motion relations." *Seism. Res. Lett.,* 68(1), 24-40.

Atkinson, G.M and W.J. Silva (1997). "An empirical study of earthquake source spectra for California earthquakes," *Bull. Seism. Soc. Am.* 87(1), 97-113.

Boore, D.M. and G.M. Atkinson (1987). "Stochastic prediction of ground motion and spectral response parameters at hard-rock sites in eastern North America," *Bull. Seism. Soc. Am.*, 77(2), 440-467.

Burns, S.E. and P.W. Mayne. (1996). "Small- and high-Strain Measurements of In-Situ Soil Properties Using the Seismic Cone Penetrometer," *Transportation Research Record* No. 1548, National Academy Press, Washington D.C., 81-88.

Campbell, K W. (1997). "Empirical near-source attenuation relationships for horizontal and vertical components of peak ground acceleration, peak ground velocity, and pseudo-absolute acceleration response spectra," *Seism. Res. Lett.,* 68(1), 154-176.

Electric Power Research Institute (1993). "Guidelines for determining design basis ground motions." Palo Alto, Calif: Electric Power Research Institute, vol. 1-5, EPRI TR-102293.
vol. 1: Methodology and guidelines for estimating earthquake ground motion in eastern North America.
vol. 2: Appendices for ground motion estimation.
vol. 3: Appendices for field investigations.
vol. 4: Appendices for laboratory investigations.
vol. 5: Quantification of seismic source effects.

Hegazy, Y.A. and P.W. Mayne (1995). "Statistical Correlations Between V_s and CPT Data for Different Soil Types," *Proceedings, Cone Penetration Testing (CPT'95),*

Vol. 2, Linköping, Sweden, 173-178.

Herrmann, R.B. (1985). "An extension of random vibration theory estimates of strong ground motion to large distance," *Bull. Seism. Soc. Am*., 75, 1447-1453.

Juang, C.H., Andrus, R.D., Jiang, T., and Chen, C.J. (2001). "Probability-based liquefaction evaluation using shear wave velocity measurements," *Proceedings, 4th International Conference on Recent Advances in Geotechnical Earthquake Engineering and Soil Dynamics*, S. Prakash, (ed.), held 26-31 March 2001, San Diego, Calif. University of Missouri at Rolla, Paper 4.25.

Juang, C.H., Chen, C.J., Jiang, T., and Andrus, R.D. (2000). "Risk-based liquefaction potential evaluation using SPT," *Canadian Geotechnical Journal*, 37, 1195-1208.

Mayne, P.W. and Rix, G.J. (1993). "G_{max}-q_c Relationships for Clays," ASTM *Geotechnical Testing Journal*, Vol. 16 (1), 54-60.

Mayne, P.W. and Rix, G.J. (1995). "Correlations Between Shear Wave Velocity and Cone Tip Resistance in Clays," *Soils and Foundations,* 35 (2), 107-110.

Rhea, S. (1984). "Q determined from local earthquakes in the South Carolina coastal plain," *Bull. Seism. Soc. Am.*, 74(6), pp. 2257-2268.

Robertson, P.K., and R.G. Campanella (1985). "Liquefaction potential of sands using the CPT," *Journal of Geotechnical Engineering*, ASCE, 111(3), 384-403.

Roblee, C.J., W.J. Silva, G.R. Toro, and N. Abrahamson (1996). "Variability in Site-Specific Seismic Ground-Motion Predictions," Uncertainty in the Geologic Environment: From Theory to Practice, *Proceedings of "Uncertainty '96" ASCE Specialty Conference*, Edited by C.D. Shackelford, P.P. Nelson, and M.J.S. Roth, Madison, WI, Aug. 1-3, pp. 1113-1133

Sadigh, K., C.-Y. Chang, J.A. Egan, F. Makdisi, and R.R. Youngs (1997). "Attenuation relationships for shallow crustal earthquakes based on California strong motion data," *Seism. Res. Lett.,* 68(1), 180-189.

Schneider, J.F., W.J. Silva, and C.L. Stark (1993). "Ground motion model for the 1989 **M** 6.9 Loma Prieta earthquake including effects of source, path and site," *Earthquake Spectra,* 9(2), 251-287.

Seed, R.B, Cetin, K.O., Moss, R.E.S., Kammerer, A.M., Wu, J., Pestana, J.M., and Riemer, M.F. (2001). "Recent advances in soil liquefaction engineering and seismic site response evaluation." *Proceedings: 4th International Conference on Recent Advances in Geotechnical Earthquake Engineering and Soil Dyanamics and Symposium in Honor of Professor W.D. Kiam Finn*, San Diego, California, March 26-31, 2001.

Seed, H.B., Idriss, I.M. and Arango, I. (1983). "Evaluation of liquefaction potential using field performance data," *J. Geotech. Engrg. Div*., ASCE, 109(3), 458-484.

Seed, H.B., and Idriss, I.M. (1982). "Ground Motions and Soil Liquefaction During Earthquakes," Earthq. Eng. Res. Inst. Monograph, Berkeley, California.

Seed, H.B., C. Ugas and J. Lysmer. (1976). "Site-dependent spectra for earthquake resistant design," *Bull. Seism. Soc. Am.*, 66(1), 221-243.

Seed, H. B. and I. M. Idriss (1971). "Simplified Procedure for Evaluating Soil Liquefaction Potential," *Journal Soil Mechanics and Foundation Division*, ASCE, 97(SM9), 1249-1273.

Silva, W.J. and C. Costantino, and Y. Iwasaki. (1999). "Assessment of liquefaction potential for the 1995 Kobe, Japan earthquake including finite-source effects." Prepared for U.S Army Engineer Waterways Experiment Station, Corps of Engineers Contract #DACW39-97-K-0015.

Silva, W.J., N. Abrahamson, G. Toro, and C. Costantino (1997). "Description and validation of the stochastic ground motion model," Submitted to Brookhaven National Laboratory, Associated Universities, Inc. Upton, New York.

Silva, W.J. and R. Darragh (1995). "Engineering characterization of earthquake strong ground motion recorded at rock sites," Palo Alto, California, Electric Power Research Institute, TR-102261.

Spudich, P., J.B. Fletcher, M. Hellweg, J. Boatwright, C. Sullivan, W.B. Joyner, T.C. Hanks, D.M. Boore, A. McGarr, L.M. Baker, and L.G. Lindh (1997). "SEA96 – A new predictive relation for earthquake ground motions in extensional tectonic regimes," *Seis. Res. Lett.,* 68(1), 190-198.

Stepp, J.C., I. Wong, J. Whitney, R. Quittmeyer, N. Abrahamson, K. Coppersmith, G. Toro, R. Yongs, J. Savy, T. Sullivan, and Yucca Mountain PSHA Project Members (2001). "Probabilistic seismic hazard analyses for ground motions and fault displacement at Yucca Mountain, Nevada," *Earthquake Spectra*, 17, 113-115.

Toro, G.R. and R.K. McGuire (1987). "An investigation into earthquake ground motion characteristics in eastern North America," *Bull. Seism. Soc. Am.*, 77(2), 468-489.

Toro, G.R., N.A. Abrahamson, and J.F. Schneider (1997). "A Model of strong ground motions from earthquakes in Central and Eastern North America: Best estimates and uncertainties," *Seism. Res. Lett.,* 68(1), 41-57.

Wong, I.G. and S.S. Olig (1998). "Seismic hazards in the Basin and Range Province: Perspectives from probabilistic analyses," in W.R. Lund (editor), Western States Seismic Policy Council, Proceedings volume, Basin and Range Province Seismic-Hazards summit. Utah Geological Survey Miscellaneous Publications 98-2, p. 110-127.

Youd, T.L., and Idriss, I.M., eds., (1997). *Proceedings of the NCEER Workshop on Evaluation of Liquefaction Resistance of Soils*, Technical Report NCEER-97-0022,

National Center for Earthquake Engineering Research, 276 p.

Youd, T.L., and Idriss, I.M., (2001). "Liquefaction resistance of soils: Summary report from the 1996 NCEER and 1998 NCEER/NSF workshop on evaluation of liquefaction resistance of soils," *Journal of Geotechnical and Geo-environmental Engineering*, ASCE, Vol. 127, No. 4, 297-313.

Table 1 CRUSTAL MODEL*		
Thickness (km)	VS (km/sec)	Density (cgs)
1.40	1.95	2.30
14.10	3.39	2.70
9.90	3.68	2.75
16.60	4.31	2.80
------	4.54	3.35

* Regional crust (Pechmann, 1999)

Table 2
POINT SOURCE RUNS

M 4.5, 5.5, 6.5, 7.5, 8.5

D(km) 1, 5, 10, 20, 50, 75, 100, 200, 400

30 simulations = 1350 runs

Randomly vary source depth, $\Delta\sigma$, kappa, Q_o, η, profile

Depth, $\sigma_{lnH} = 0.6$, $\overline{H}$ (**M** > 5) = 8 km; Source Utah Seismicity

M	Lower Bound (km)	-2σ (km)	-σ (km)	$\overline{H}$ (km)	σ (km)	2σ (km)	Upper Bound (km)
4.5	4	2	3	7.5	11	20	12
5.5	4	2	3	7.5	11	20	12
6.5	5	2	4	7.5	14	27	10
7.5	5	3	5	7.5	18	33	10
8.5	5	3	5	7.5	18	33	10

$\Delta\sigma$, $\sigma_{ln\Delta\sigma} = 0.5$, Based on California earthquake inversions (Silva et al., 1997)

M	$\Delta\sigma$ (bars)	AVG. $\Delta\sigma$ (bars) = 46
4.5	60	Based on inversions of the Abrahamson and Silva (1997) empirical attenuation relation for normal source mechanisms
5.5	60	
6.5	45	
7.5	36	
8.5	36	

$Q(s)$, $\overline{Q_o} = 370$, $\sigma_{\ln Q_o} = 0.40$

$\eta = 0.35$, $\sigma_\eta = 0.$

Vary Q_o sufficient, $\pm 1\ \sigma$ covers range of Southern California inversions from 1 to 20 Hz

Kappa, $\overline{\kappa} = 0.04$ sec (EPRI, 1993) $\sigma_{ln\kappa} = 0.3$ (EPRI, 1993)

Profile, Geomatrix C + D over Salt Lake City crust

Geometrical attenuation $R^{-(a + b\,\mathbf{M})}$, a = 1.0296, b = -0.0422 (Silva et al., 1997)
$R^{-(a + b\,\mathbf{M})/2}$, R > 70 km

Table 3

REGRESSION COEFFICIENTS[1] FOR GROUND MOTIONS AND LIQUEFACTION PARAMETERS USING THE EPRI SOIL CURVES

Freq. (Hz)	C1	C2	C4	C6	C7	C10	Param. Sigma	Total Sigma
0.20	-15.75303	2.32273	1.70	-1.05196	0.00915	-0.39204	0.4135	1.2087
0.40	-10.42347	1.76950	2.00	-1.42607	0.04955	-0.36599	0.5182	1.0644
0.50	-8.15874	1.50687	2.20	-1.64803	0.07566	-0.34228	0.4982	0.9975
0.60	-6.60794	1.32222	2.30	-1.79260	0.09277	-0.32311	0.4526	0.9144
1.00	-2.05205	0.77650	2.60	-2.30947	0.15155	-0.26184	0.4726	0.8140
1.30	0.39698	0.47898	2.80	-2.60448	0.18338	-0.22647	0.5242	0.8439
2.00	4.45838	0.02001	3.10	-3.15328	0.23940	-0.18032	0.5042	0.7760
2.50	6.93859	-0.23922	3.30	-3.53642	0.27569	-0.16565	0.4828	0.7430
3.00	8.79052	-0.45561	3.40	-3.83849	0.30808	-0.15253	0.5062	0.7601
4.00	11.06792	-0.71902	3.50	-4.22718	0.34881	-0.13550	0.5182	0.7468
5.00	13.27845	-0.97822	3.60	-4.61207	0.39124	-0.12106	0.5172	0.7340
6.00	13.89172	-1.07057	3.60	-4.71941	0.40482	-0.11059	0.5170	0.7261
7.00	14.23706	-1.12354	3.60	-4.80003	0.41444	-0.10379	0.5126	0.7234
8.00	14.46434	-1.16154	3.60	-4.86144	0.42227	-0.09911	0.5074	0.7256
10.00	13.38660	-1.08171	3.50	-4.71060	0.41072	-0.09331	0.4936	0.7024
12.00	12.16742	-0.97172	3.40	-4.53025	0.39437	-0.09274	0.4770	0.6831
14.00	10.92298	-0.85244	3.30	-4.33409	0.37557	-0.09380	0.4737	0.6799
16.00	9.78122	-0.74124	3.20	-4.15494	0.35853	-0.09677	0.4645	0.6763
18.00	9.44006	-0.69764	3.20	-4.10846	0.35252	-0.09984	0.4597	0.6689
20.00	9.12528	-0.65668	3.20	-4.06447	0.34682	-0.10319	0.4549	0.6680
25.00	7.85649	-0.52326	3.10	-3.85918	0.32584	-0.10950	0.4475	0.6597
31.00	7.46987	-0.47187	3.10	-3.80092	0.31826	-0.11412	0.4422	0.6521
40.00	7.18487	-0.43351	3.10	-3.75760	0.31259	-0.11793	0.4384	0.6458
50.00	7.06076	-0.41675	3.10	-3.73869	0.31011	-0.11967	0.4368	0.6466
100.00	6.32803	-0.35124	3.00	-3.61250	0.29902	-0.12104	0.4355	0.6462
PGA	6.35980	-0.35514	3.00	-3.61086	0.29868	-0.11903	0.4355	0.6462
PGV	2.82644	0.71431	2.30	-2.45805	0.17255	-0.19763	0.4088	---
CSR	5.47559	-0.26377	3.00	-3.50099	0.28584	-0.12274	0.4226	---
FS	-2.58163	-0.31972	2.90	3.36561	-0.27171	0.22636	0.6825	---
Prob. of Liquef.	18.67064	-0.34019	3.10	-13.74106	1.25502	-0.97136	2.5134	---

[1]Regression coefficients C5 and C8 are equal to 0.0.

Table 4
REGRESSION COEFFICIENTS[1] FOR GROUND MOTIONS AND LIQUEFACTION PARAMETERS USING THE PENINSULA RANGE SOIL CURVES

Freq. (Hz)	C1	C2	C4	C6	C7	C10	Param. Sigma	Total Sigma
0.20	-15.62614	2.29657	1.70	-1.06964	0.01308	-0.39205	0.4096	1.2074
0.40	-10.60906	1.80268	2.00	-1.38378	0.04191	-0.36304	0.5329	1.0716
0.50	-8.59539	1.56578	2.10	-1.56148	0.06384	-0.33974	0.5164	1.0067
0.60	-7.19537	1.40834	2.20	-1.67600	0.07540	-0.31758	0.4664	0.9214
1.00	-3.12588	0.95237	2.50	-2.10518	0.11773	-0.25699	0.4727	0.8140
1.30	-0.68877	0.66403	2.70	-2.40876	0.14996	-0.22234	0.5362	0.8514
2.00	3.07402	0.25666	3.00	-2.90602	0.19704	-0.17422	0.4928	0.7687
2.50	4.68008	0.08660	3.10	-3.13481	0.21725	-0.15770	0.4637	0.7308
3.00	6.35012	-0.10288	3.20	-3.41199	0.24614	-0.14665	0.4928	0.7512
4.00	8.36990	-0.32727	3.30	-3.75592	0.27998	-0.13155	0.5077	0.7395
5.00	11.37739	-0.64429	3.50	-4.28679	0.33395	-0.12134	0.5087	0.7280
6.00	12.16677	-0.76344	3.50	-4.42681	0.35271	-0.11154	0.5107	0.7216
7.00	12.60762	-0.82876	3.50	-4.52382	0.36450	-0.10621	0.5117	0.7228
8.00	12.02297	-0.80710	3.40	-4.44758	0.36235	-0.10290	0.5127	0.7293
10.00	11.35467	-0.78350	3.30	-4.36663	0.36060	-0.09821	0.5071	0.7119
12.00	10.42609	-0.71646	3.20	-4.23288	0.35117	-0.09630	0.4925	0.6941
14.00	10.13502	-0.68906	3.20	-4.19961	0.34787	-0.09635	0.4902	0.6915
16.00	9.10575	-0.59756	3.10	-4.03828	0.33392	-0.09786	0.4798	0.6869
18.00	8.77319	-0.55832	3.10	-3.99246	0.32845	-0.10002	0.4754	0.6798
20.00	7.79524	-0.46612	3.00	-3.83114	0.31357	-0.10253	0.4701	0.6784
25.00	7.21340	-0.39286	3.00	-3.74457	0.30278	-0.10787	0.4621	0.6697
31.00	6.77608	-0.33690	3.00	-3.67679	0.29426	-0.11210	0.4553	0.6611
40.00	5.83510	-0.24439	2.90	-3.51698	0.27898	-0.11604	0.4496	0.6535
50.00	5.67083	-0.22267	2.90	-3.49090	0.27563	-0.11805	0.4469	0.6535
100.00	5.54060	-0.20563	2.90	-3.47075	0.27306	-0.11966	0.4449	0.6525
PGA	5.56562	-0.20965	2.90	-3.46815	0.27279	-0.11787	0.4443	0.6522
PGV	2.93979	0.71039	2.30	-2.47236	0.17232	-0.19704	0.4223	---
CSR	4.18368	-0.09933	2.80	-3.26828	0.25703	-0.12572	0.4227	---
FS	-2.38163	-0.34418	2.80	3.26077	-0.25619	0.15872	0.7592	---
Prob. of Liquef.	22.31569	-1.07126	3.00	-14.08721	1.33966	-0.70714	2.6417	---

[1]Regression coefficients C5 and C8 are equal to 0.0.

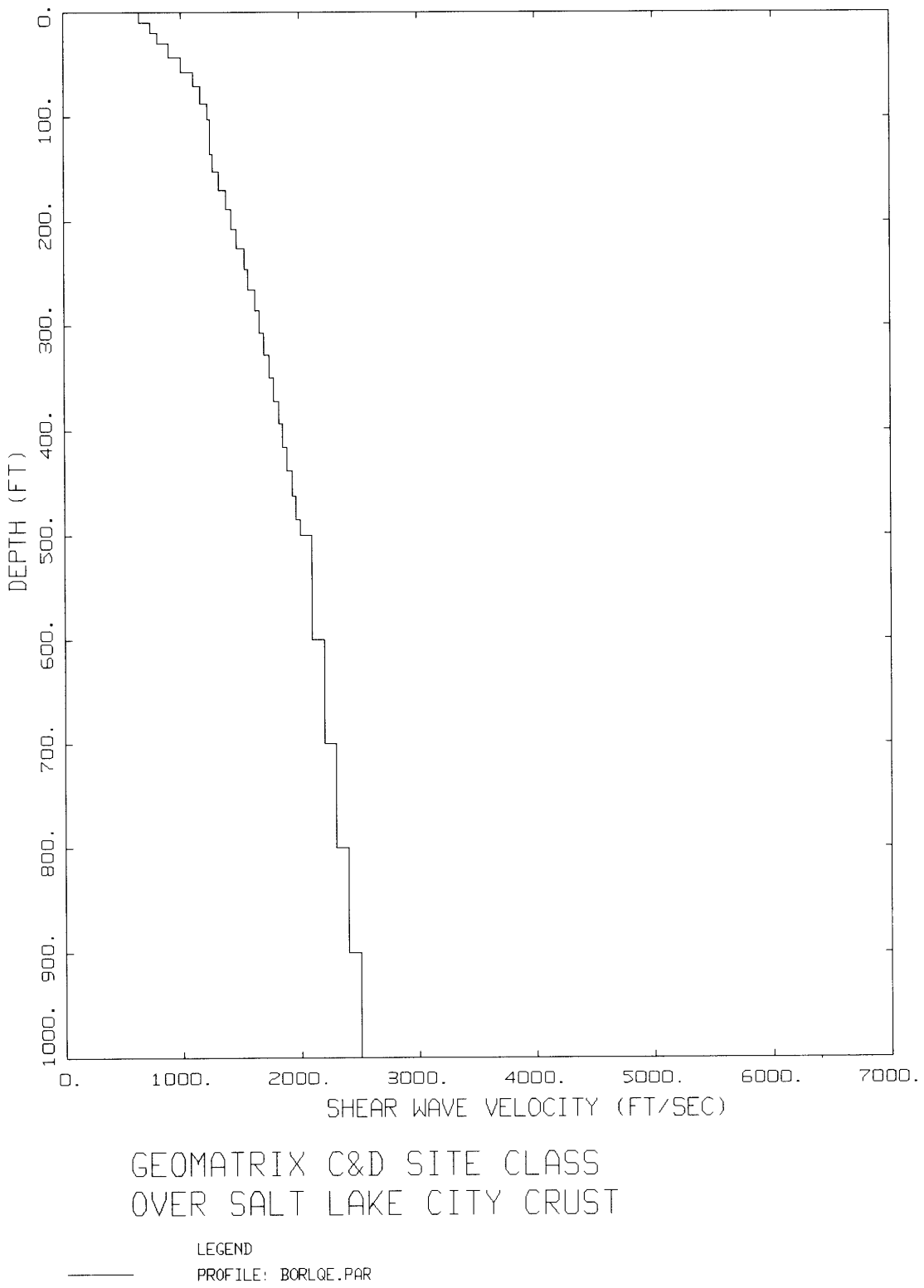

Figure 1. Base case shear-wave velocity profile model developed based on Geomatrix C and D sites.

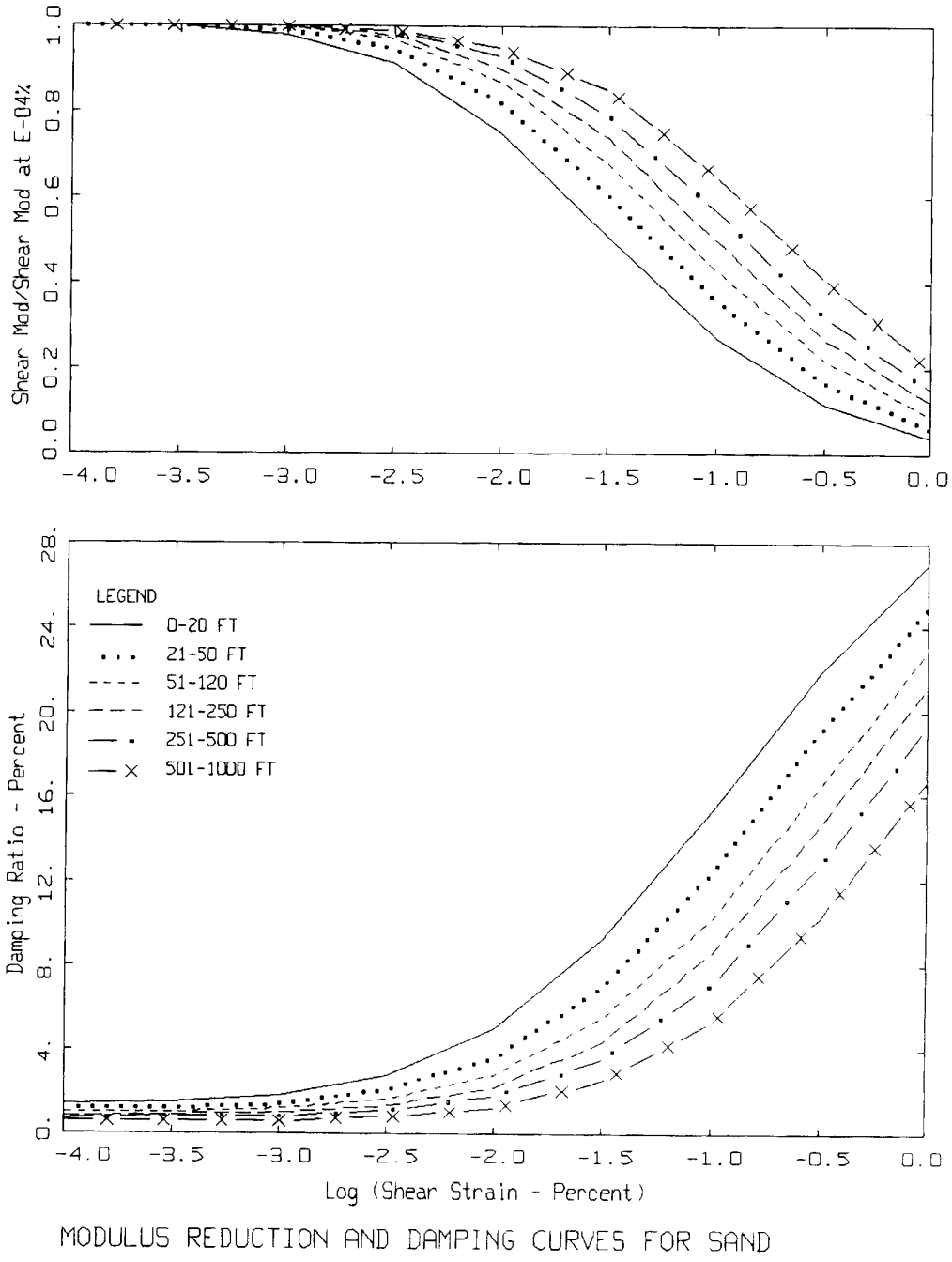

Figure 2a. Base case G/Gmax and hysteretic damping curves for cohesionless soils (EPRI 1993).

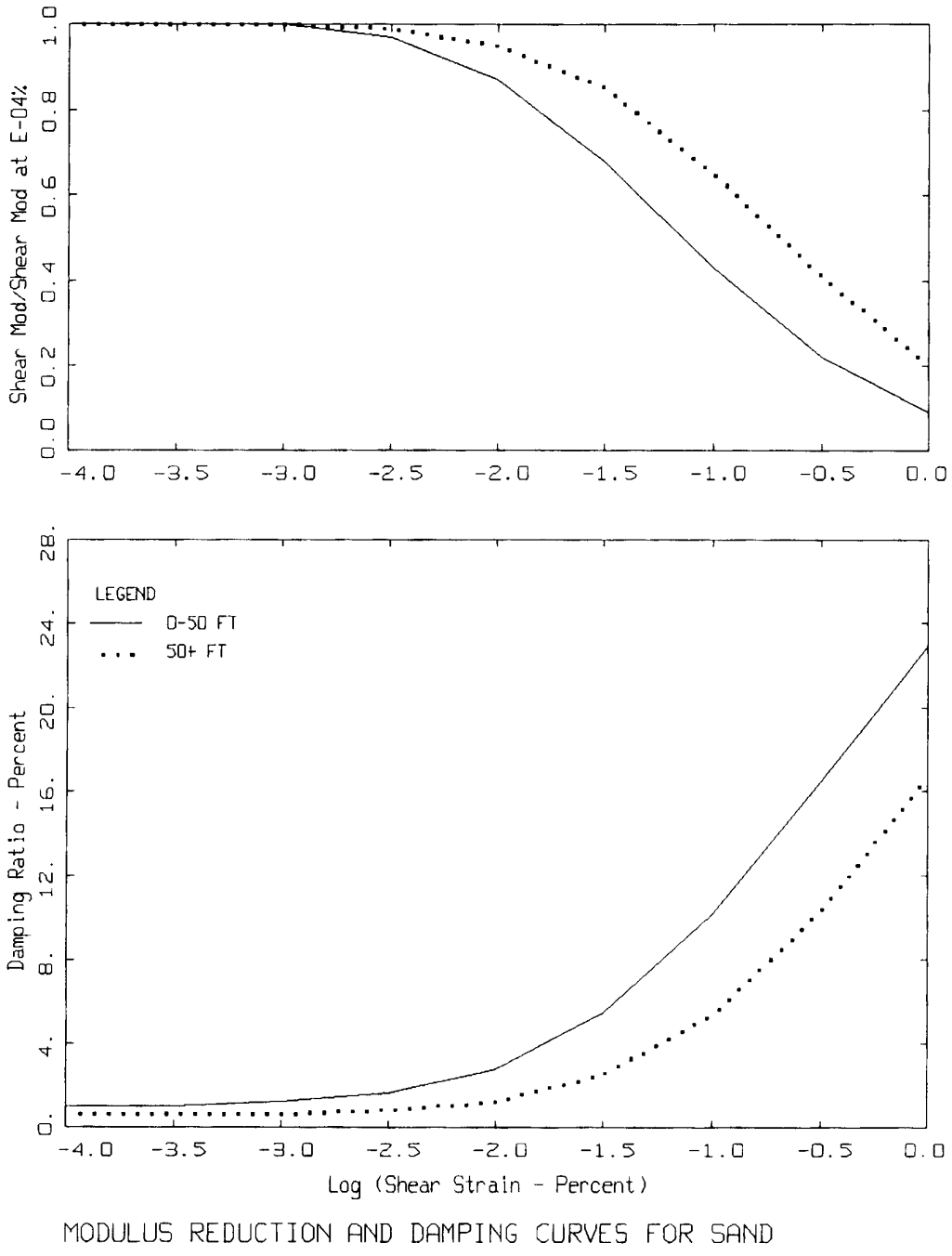

Figure 2b. Peninsula Range base case G/Gmax and hysteretic damping curves.

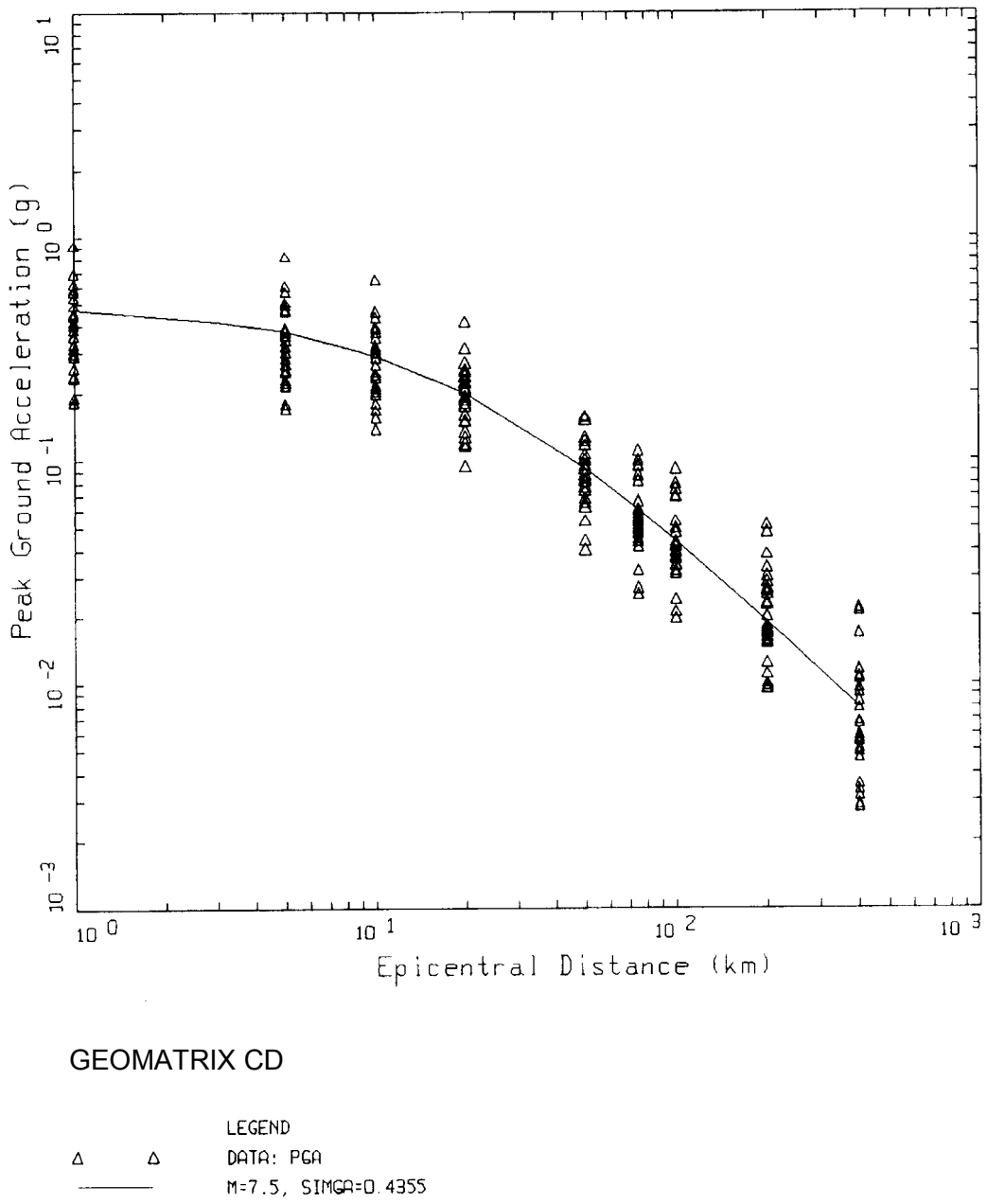

Figure 3. Peak acceleration estimates and regression fit at **M** 7.5 (EPRI soil curves).

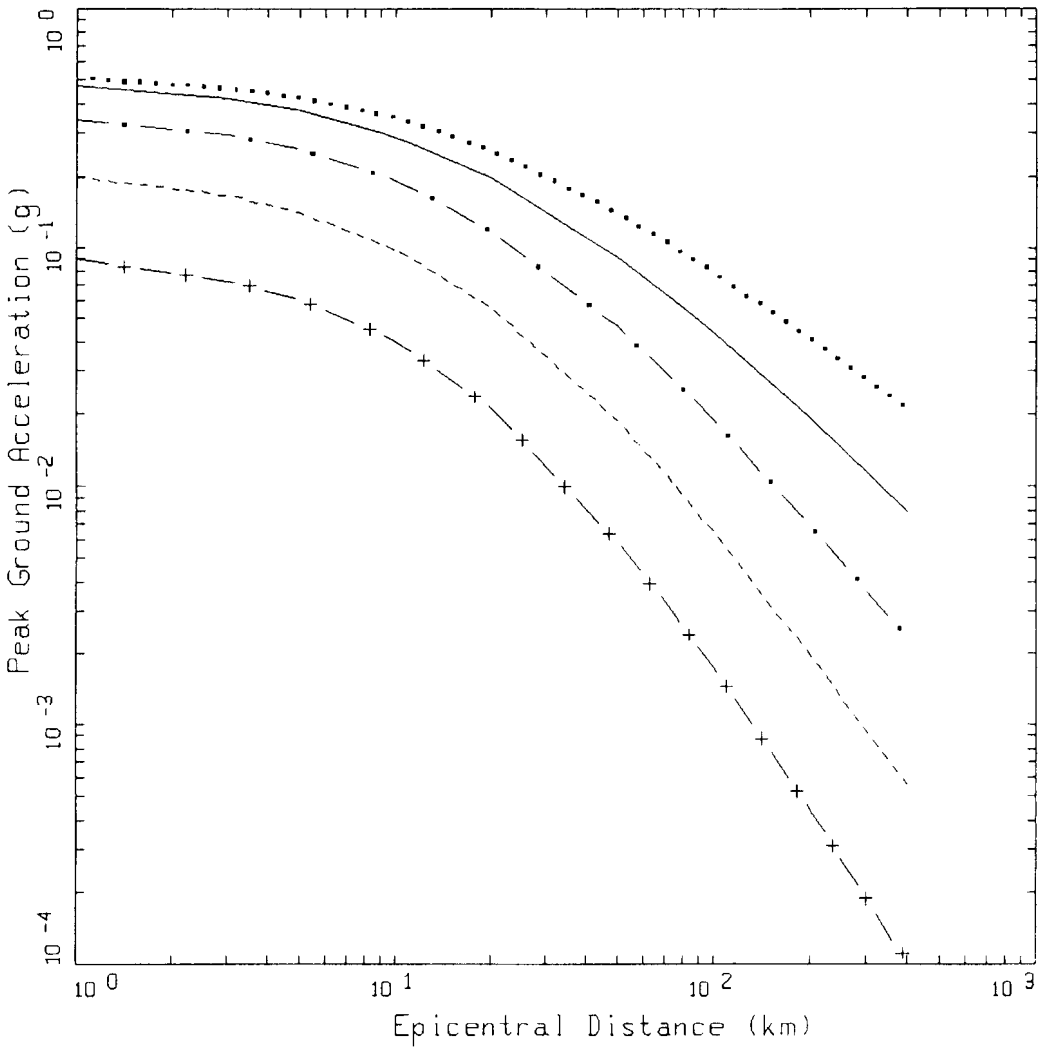

GEOMATRIX CD

LEGEND

M=4.5, SIMGA=0.4355

M=5.5, SIGMA=0.4355

M=6.5, SIGMA=0.4355

M=7.5, SIMGA=0.4355

M=8.5, SIMGA=0.4355

Figure 4. Attenuation of median peak horizontal accelerations (PGA) at **M**=4.5, 5.5, 6.5, 7.5, and 8.5 (EPRI soil curves).

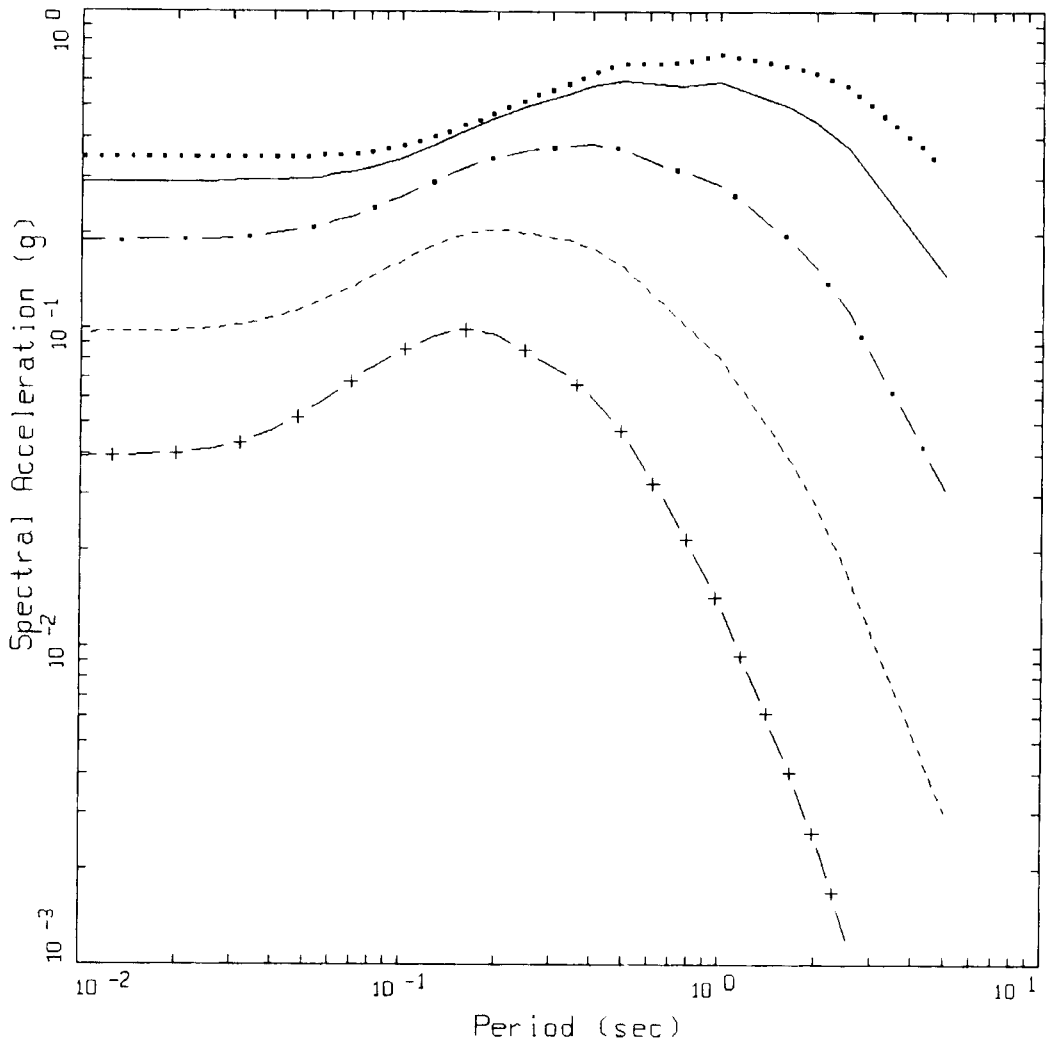

Figure 5. Median response spectra (5% damping) at a distance of 10 km for magnitudes **M**=4.5, 5.5, 6.5, 7.5, and 8.5 (EPRI soil curves).

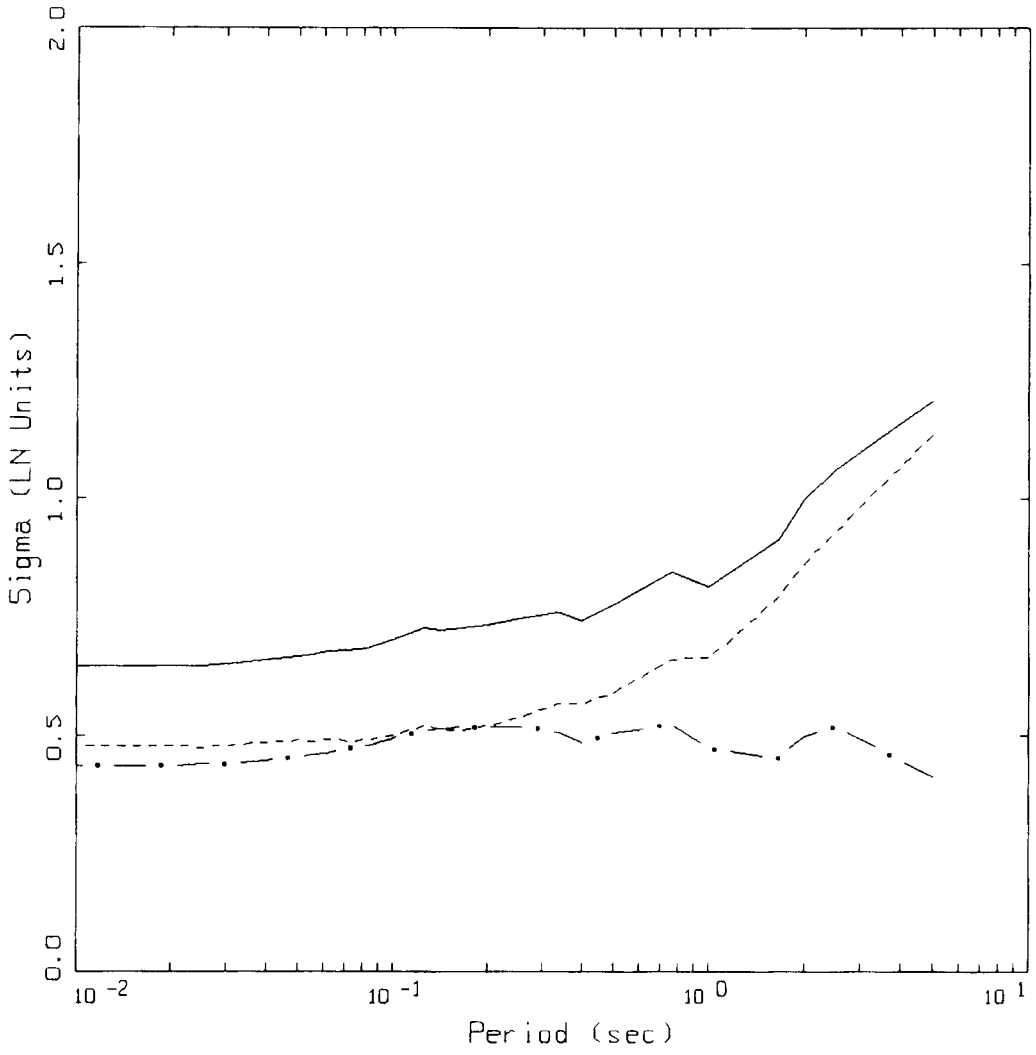

Figure 6. Estimates of total variability (uncertainty) for the attenuation model (EPRI soil curves). Parametric variability is due to variation of point source parameters (see Table 2) and fit of regression model (see Table 3). Model variability is from validation exercises with 16 earthquakes (**M** 5.3 to 7.4) at 500 sites over the fault distance range of 1 to 460 km (Appendix A).

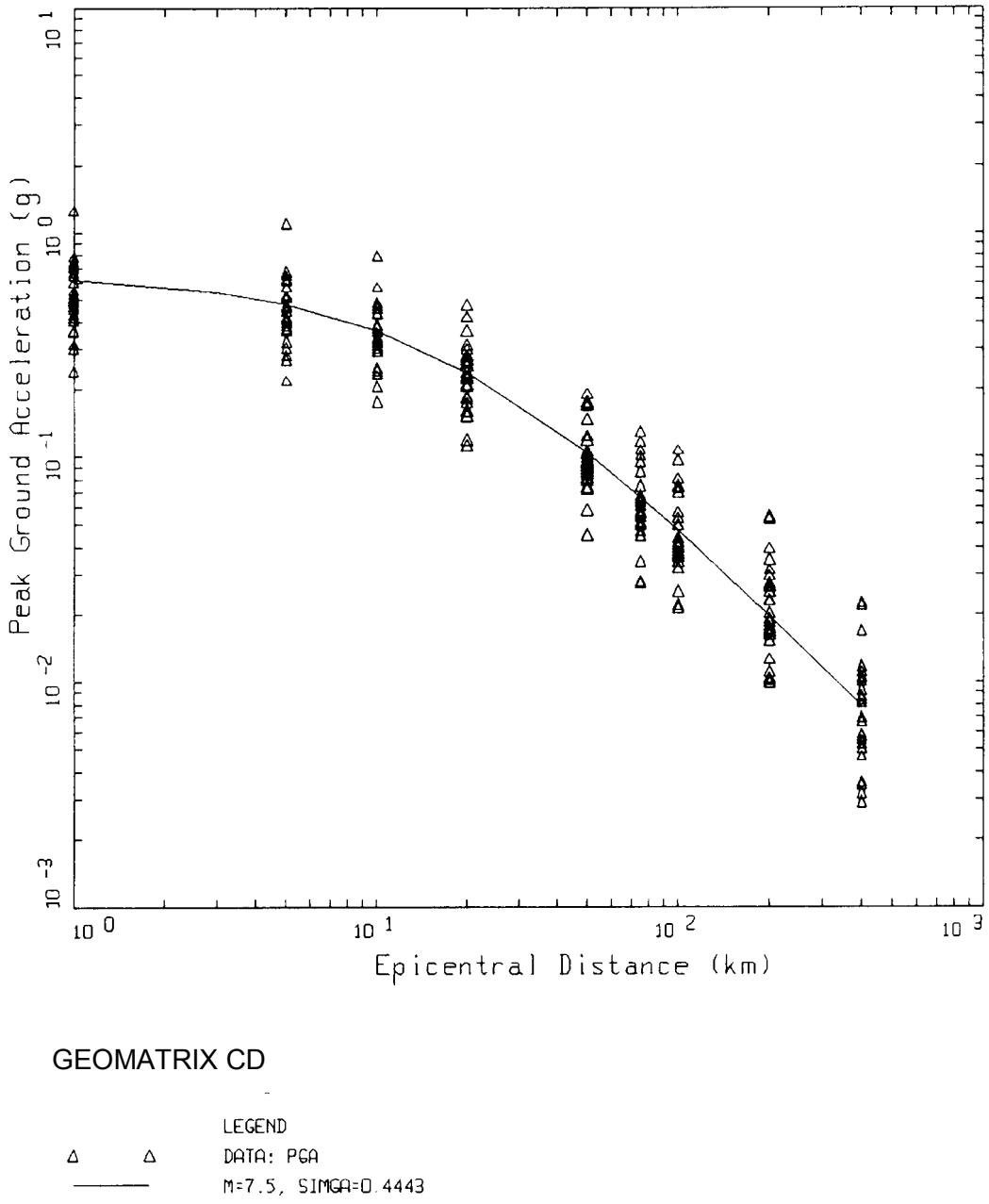

Figure 7. Peak acceleration estimates and regression fit at **M** 7.5 (Peninsula Range soil curves).

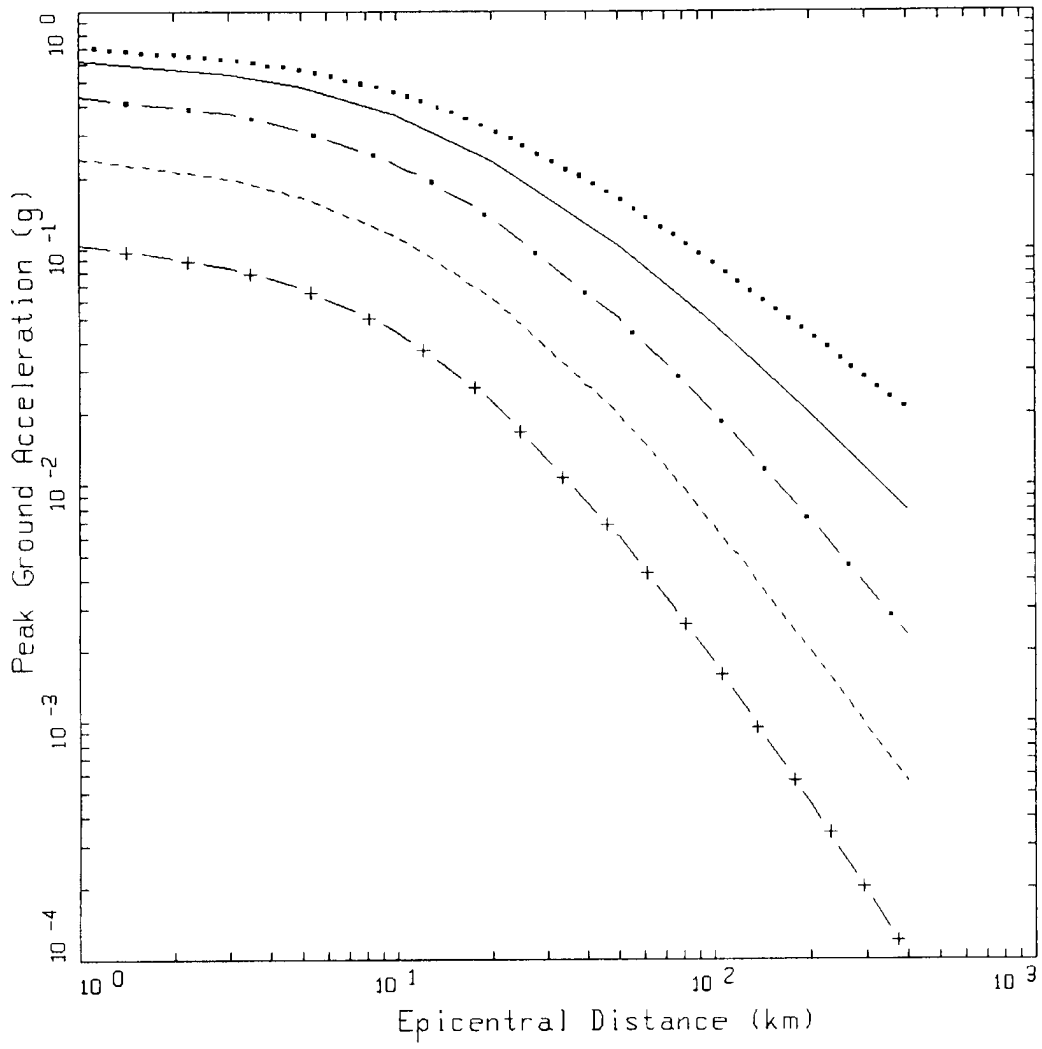

Figure 8. Attenuation of median peak horizontal accelerations (PGA) at **M**=4.5, 5.5, 6.5, 7.5, and 8.5 (Peninsula Range soil curves).

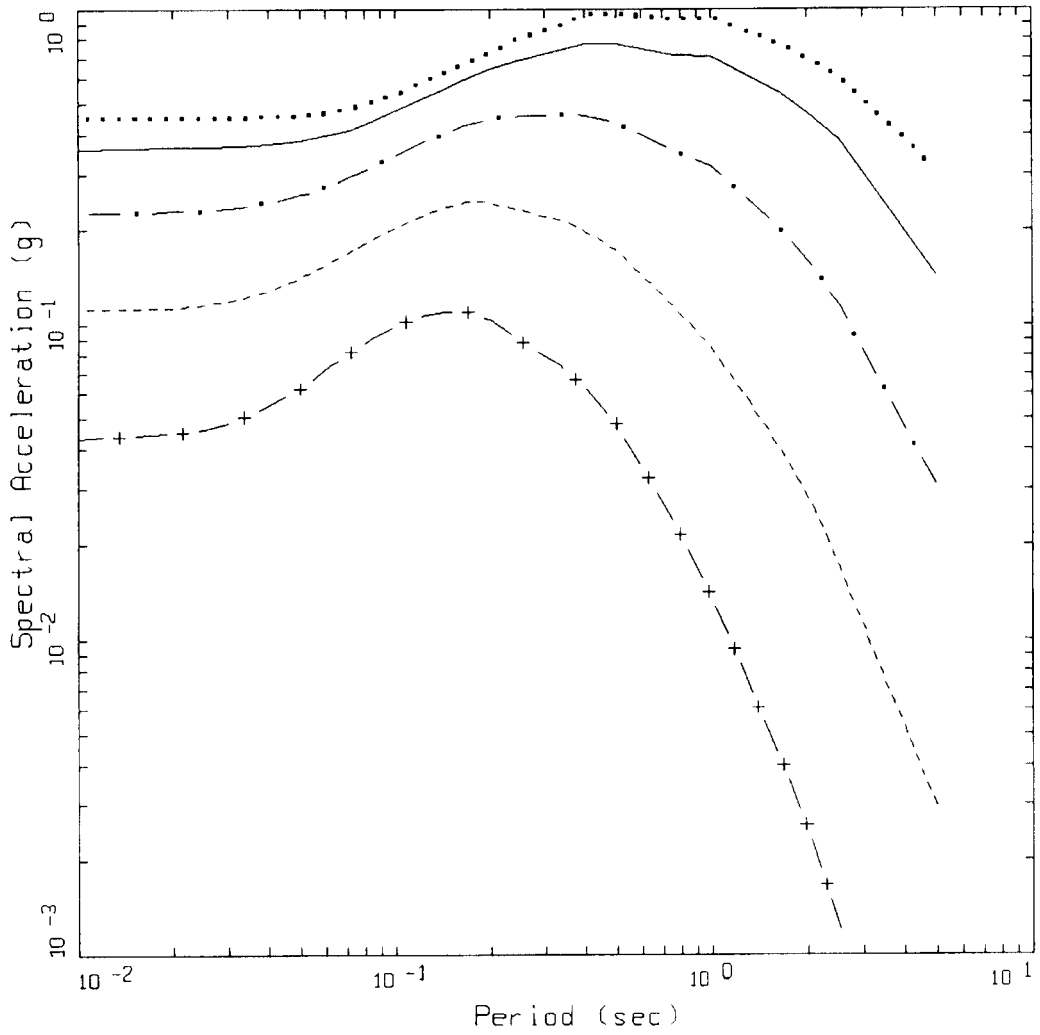

Figure 9. Median response spectra (5% damping) at a distance of 10 km for magnitudes **M**=4.5, 5.5, 6.5, 7.5, and 8.5 (Peninsula Range soil curves).

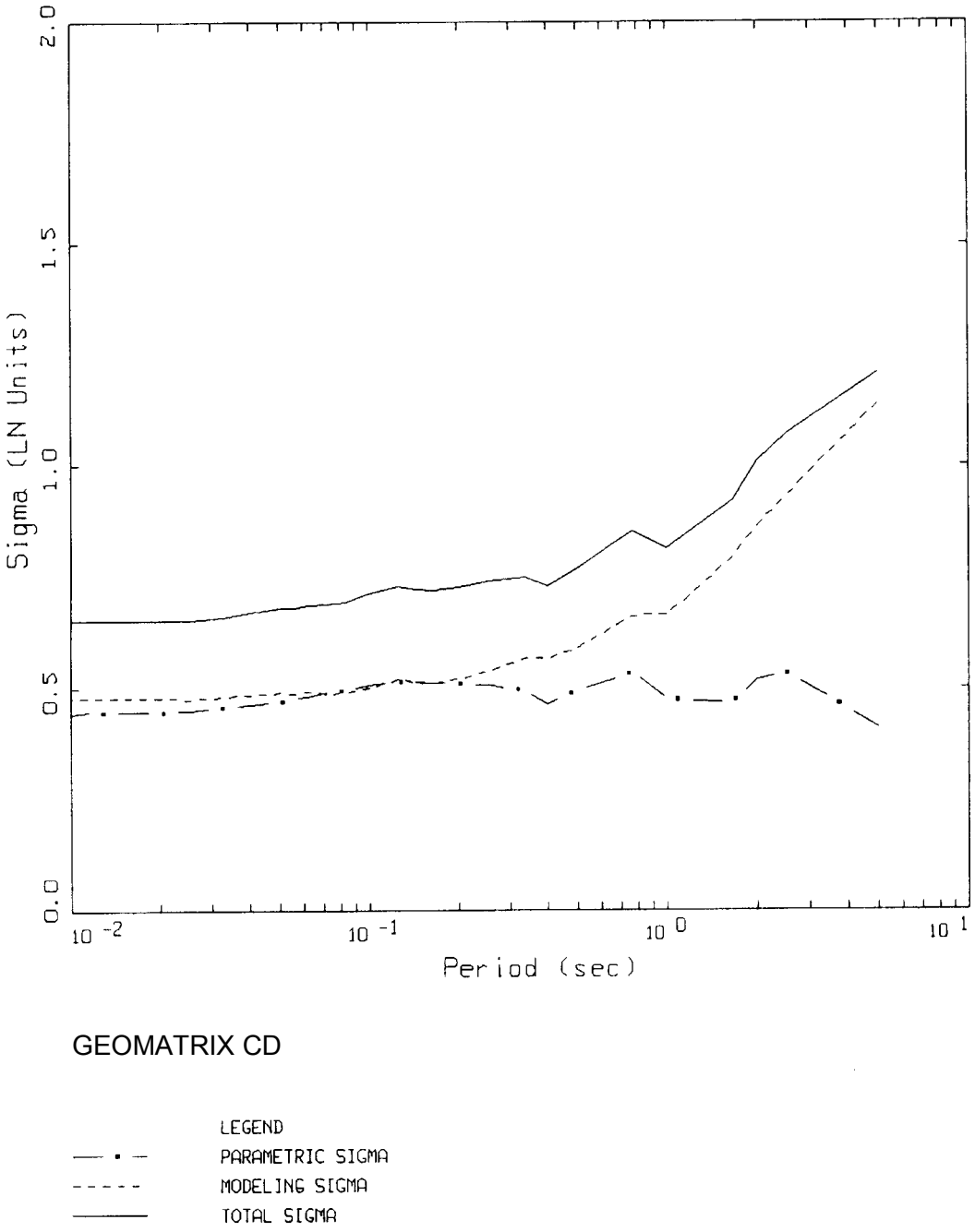

Figure 10. Estimates of total variability (uncertainty) for the attenuation model (Peninsula Range soil curves). Parametric variability is due to variation of point source parameters (see Table 2) and fit of regression model (see Table 3). Model variability is from validation exercises with 16 earthquakes (**M** 5.3 to 7.4) at 500 sites over the fault distance range of 1 to 460 km (Appendix A).

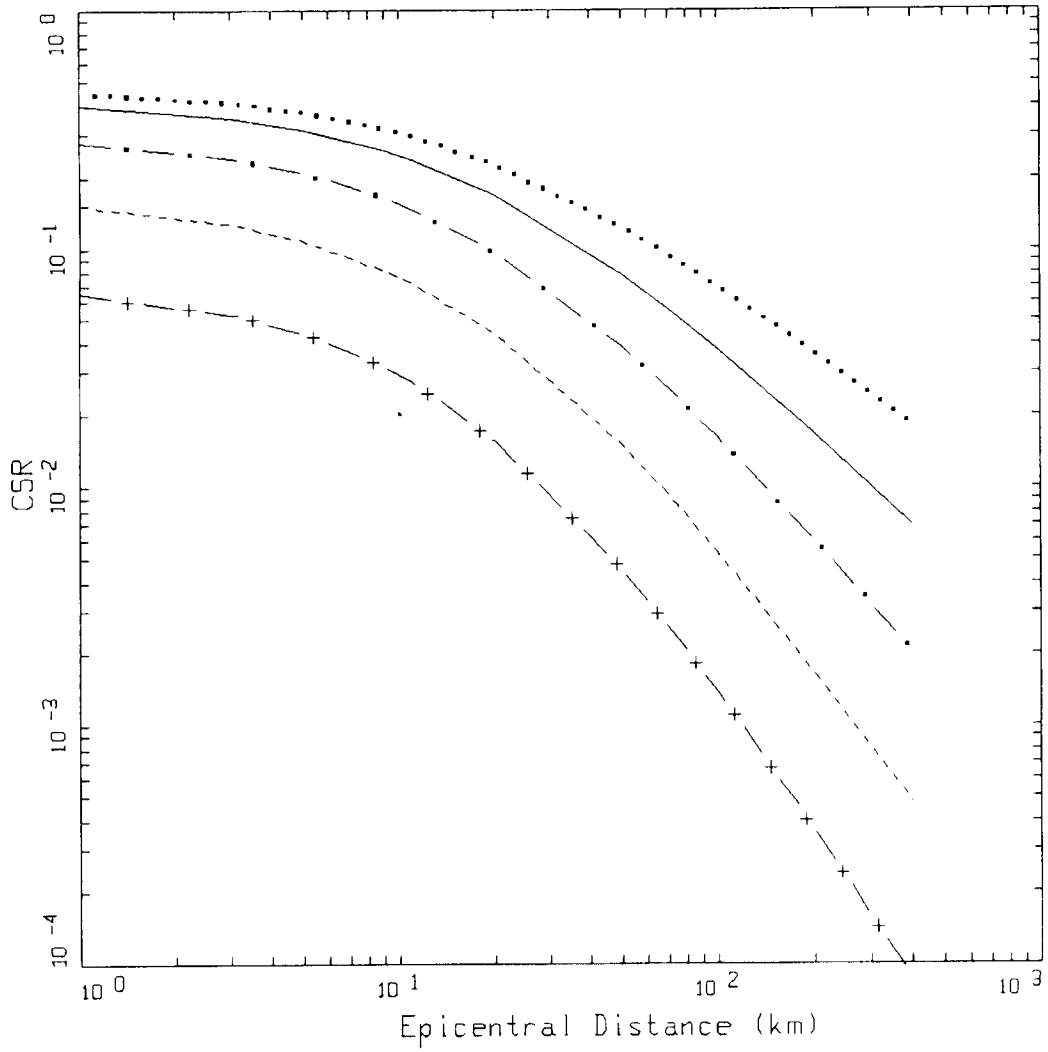

Figure 11. Attenuation of CSR parameter at **M**=4.5, 5.5, 6.5, 7.5, and 8.5 (EPRI soil curves).

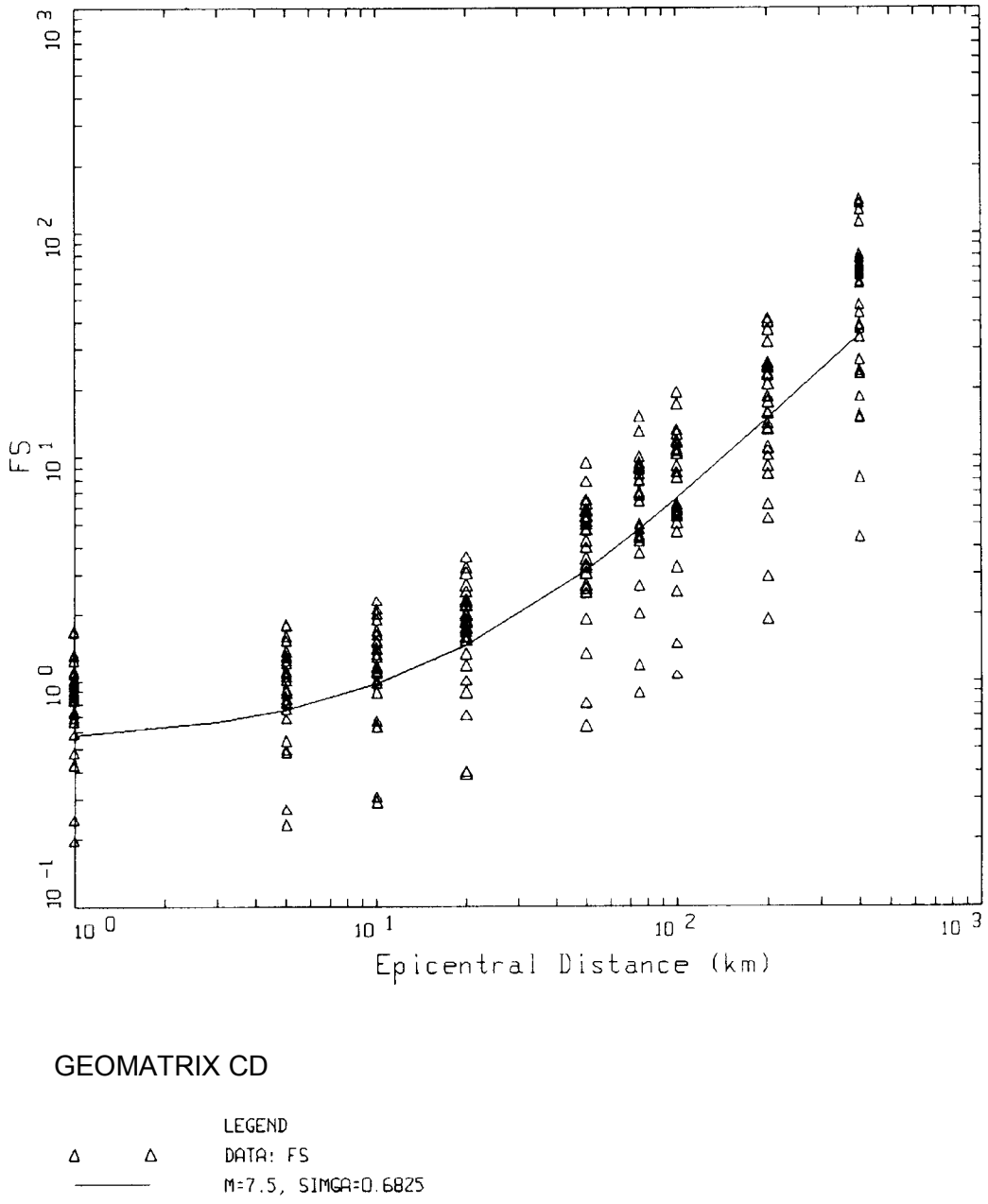

Figure 12. Factor of Safety (FS) estimates and regression fit at **M** 7.5 (EPRI soil curves).

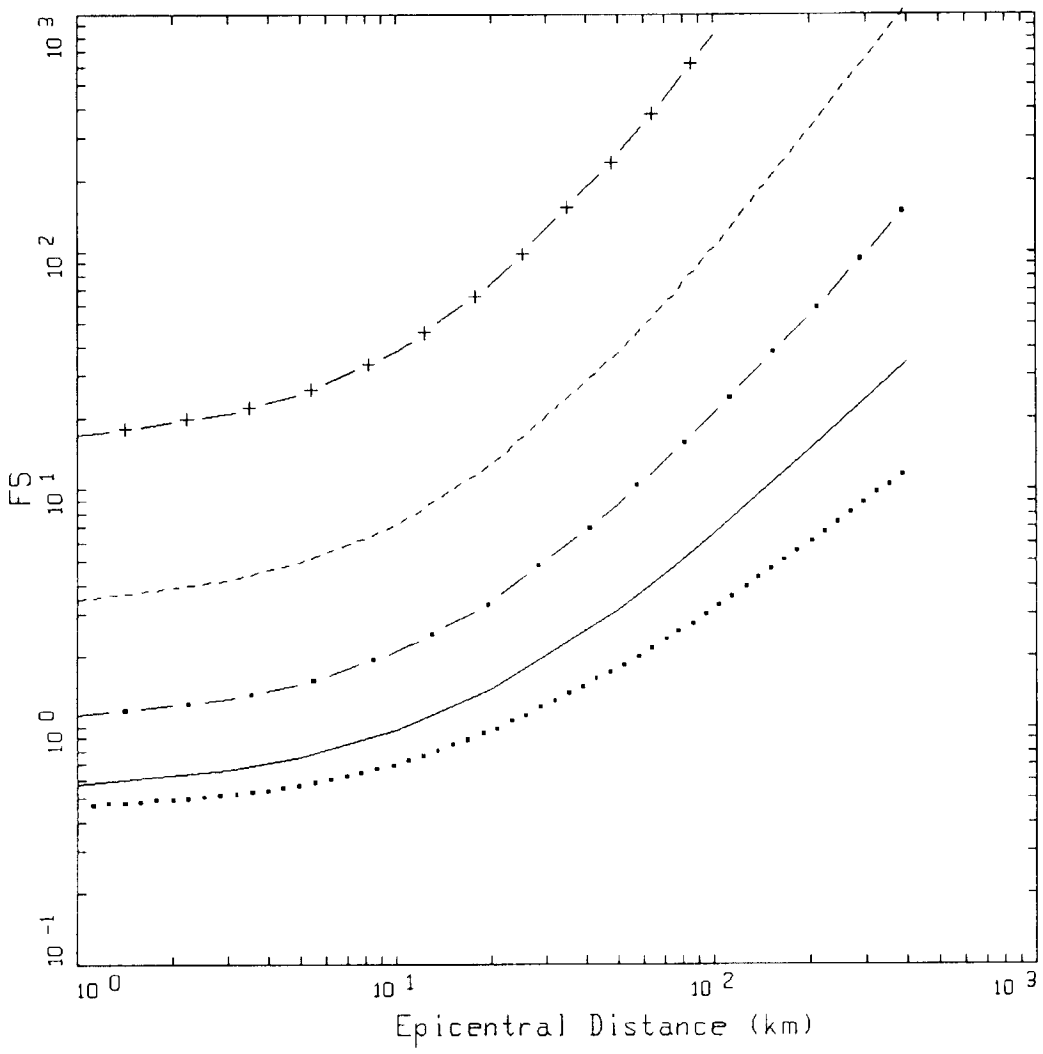

Figure 13. Attenuation of Factor of Safety (FS) parameter at **M**=4.5, 5.5, 6.5, 7.5, and 8.5 (EPRI soil curves).

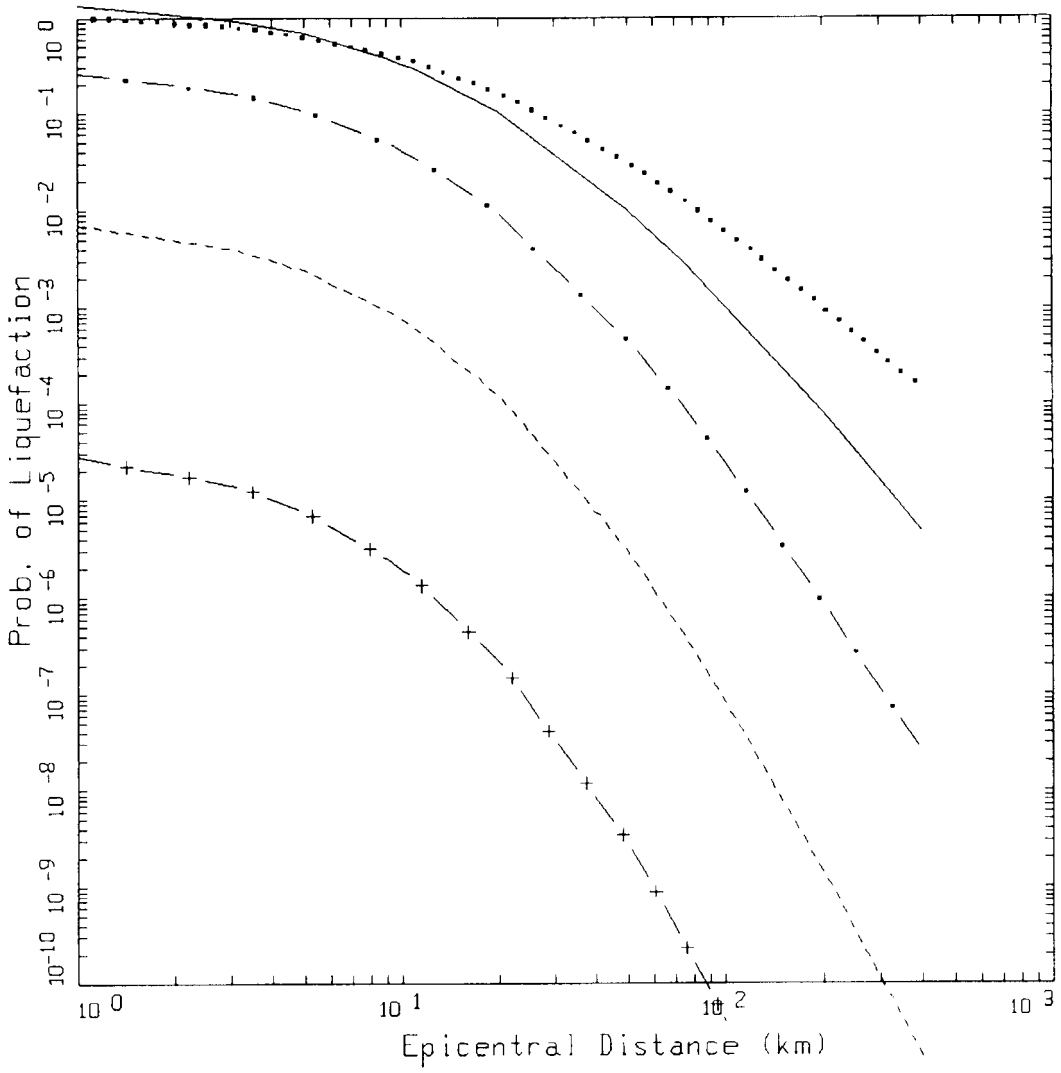

Figure 14. Attenuation of probability of liquefaction at **M**=4.5, 5.5, 6.5, 7.5, and 8.5 (EPRI soil curves).

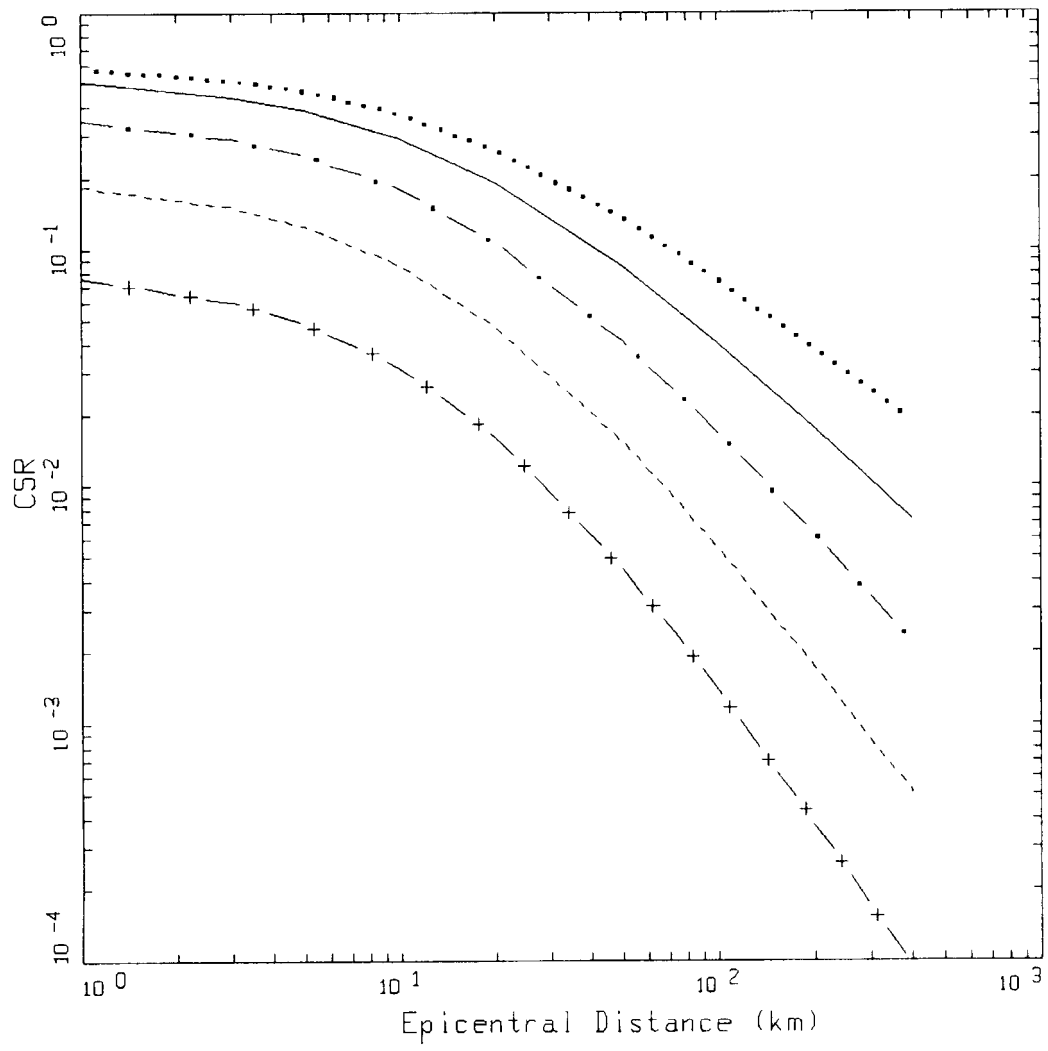

Figure 15. Attenuation of CSR parameter at **M**=4.5, 5.5, 6.5, 7.5, and 8.5 (Peninsula Range soil curves).

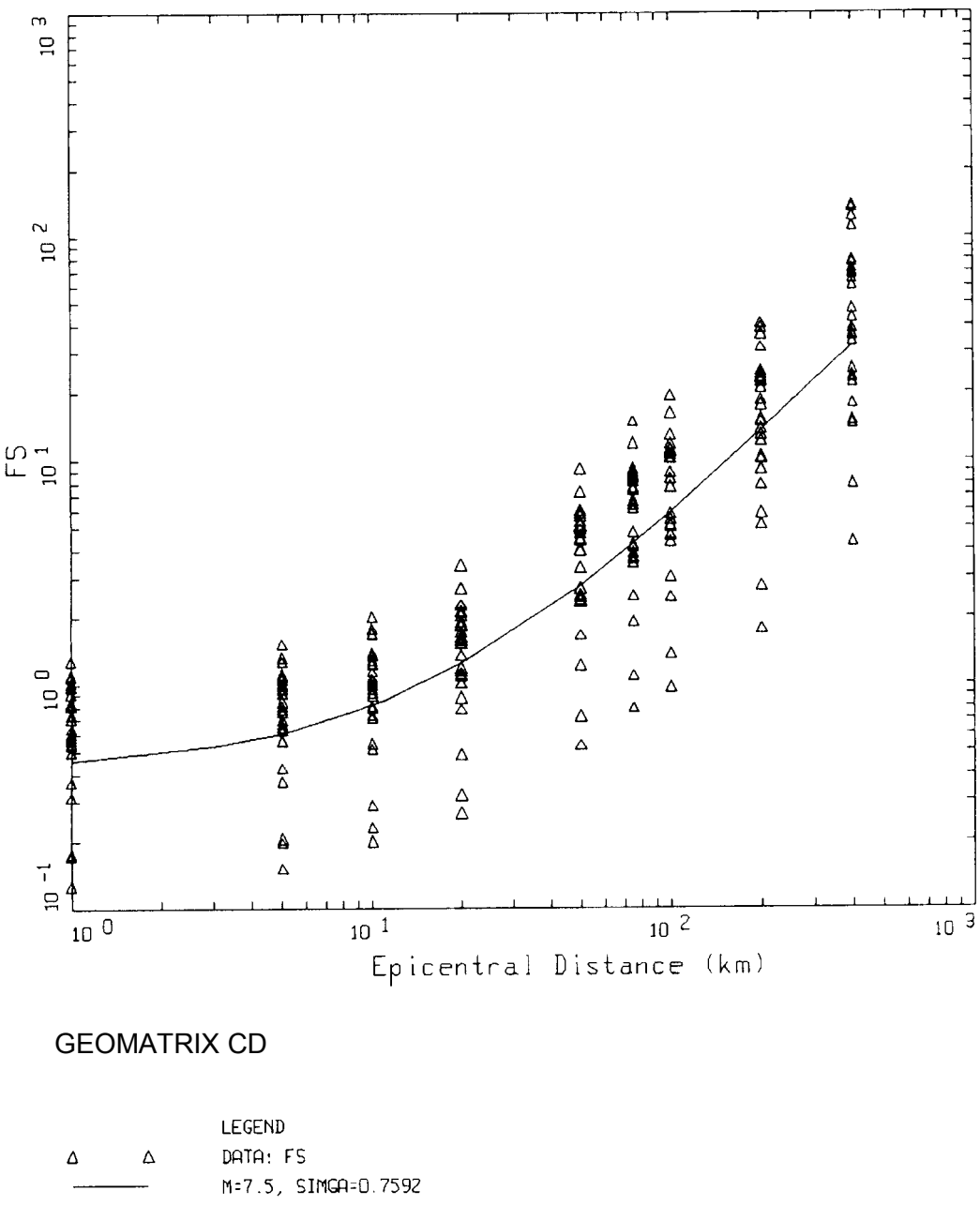

Figure 16. Factor of Safety (FS) estimates and regression fit at **M** 7.5 (Peninsula Range soil curves).

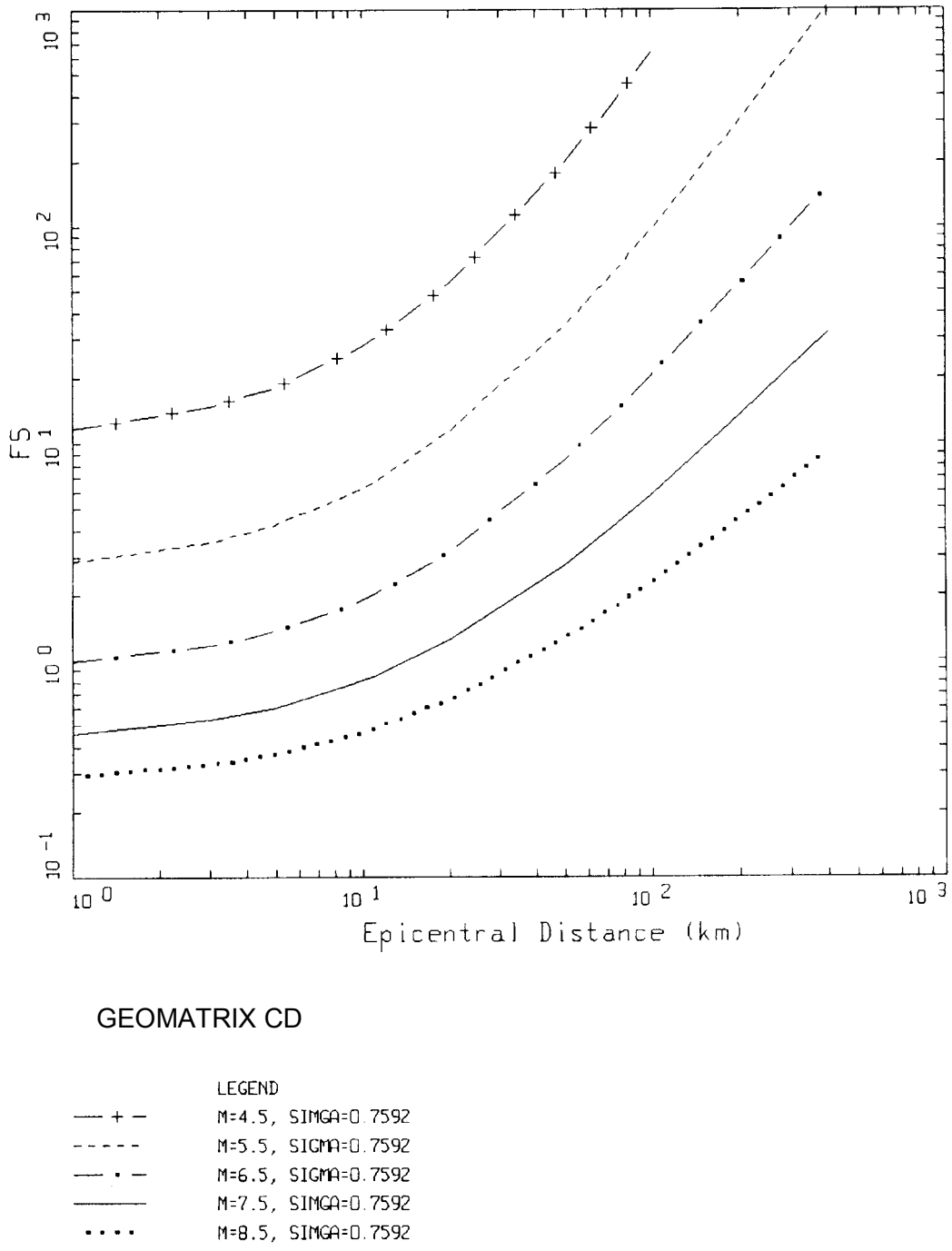

Figure 17. Attenuation of Factor of Safety (FS) parameter at **M**=4.5, 5.5, 6.5, 7.5, and 8.5 (Peninsula Range soil curves).

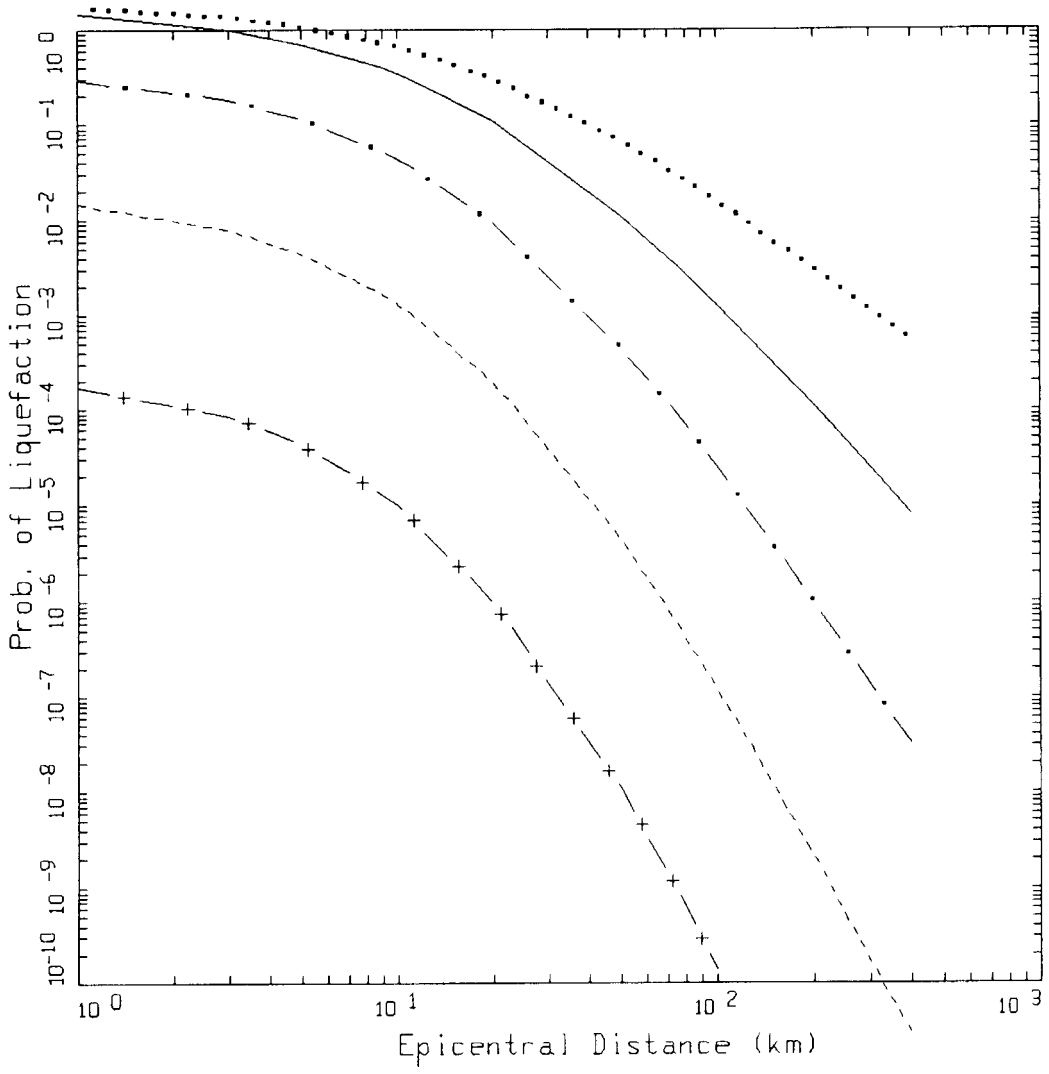

Figure 18. Attenuation of probability of liquefaction at **M**=4.5, 5.5, 6.5, 7.5, and 8.5 (Peninsula Range soil curves).

APPENDIX A

STOCHASTIC GROUND MOTION MODEL DESCRIPTION

Background

In the context of strong ground motion, the term "stochastic" can be a fearful concept to some and may be interpreted to represent a fundamentally incorrect or inappropriate model (albeit the many examples demonstrating that it works well; Boore, 1983, 1986). To allay any initial misgivings, a brief discussion seems prudent to explain the term stochastic in the stochastic ground motion model.

The stochastic point-source model may be termed a spectral model in that it fundamentally describes the Fourier amplitude spectral density at the surface of a half-space (Hanks and McGuire, 1981). The model uses a Brune (1970, 1971) omega-square description of the earthquake source Fourier amplitude spectral density. This model is easily the most widely used and qualitatively validated source description available. Seismic sources ranging from **M** = -6 (hydrofracture) to **M** = 8 have been interpreted in terms of the Brune omega-square model in dozens of papers over the last 30 years. The general conclusion is that it provides a reasonable and consistent representation of crustal sources, particularly for tectonically active regions such as plate margins. A unique phase spectrum can be associated with the Brune source amplitude spectrum to produce a complex spectrum which can be propagated using either exact or approximate (1-2- or 3-D) wave propagation algorithms to produce single or multiple component time histories. In this context the model is not stochastic, it is decidedly deterministic and as exact and rigorous as one chooses. A two-dimensional array of such point-sources may be appropriately located on a fault surface (area) and fired with suitable delays to simulate rupture propagation on an extended rupture plane. As with the single point-source, any degree of rigor may be used in the wave propagation algorithm to produce multiple component or average horizontal component time histories. The result is a kinematic[1] finite-source model which has as its basis a source time history defined as a Brune pulse whose Fourier amplitude spectrum follows an omega-square model. This finite-fault model would be very similar to that used in published inversions for slip models if the 1-D propagation were treated using a reflectivity algorithm (Aki and Richards, 1980). This algorithm is a complete solution to the wave equation from static offsets (near-field terms) to an arbitrarily selected high frequency cutoff (generally 1-2 Hz).

Alternatively, to model the wave propagation more accurately, recordings of small earthquakes at the site of interest and with source locations distributed along the fault of interest may be used as empirical Green functions (Hartzell, 1978). To model the design earthquake, the empirical Green functions are delayed and summed in a manner to simulate rupture propagation (Hartzell, 1978). Provided a sufficient number of small earthquakes are recorded at the site of interest, the source locations adequately cover the expected rupture surface, and sufficient low frequency energy is present in the Green functions, this would be the most appropriate procedure to use if nonlinear site response is not an issue. With this approach the wave propagation is, in principle, exactly represented from each Green function source to the site. However, nonlinear site response is not treated unless Green function motions are recorded at a nearby rock outcrop with dynamic material properties similar to the rock underlying the soils at the site or recordings are made at depth within the site soil column. These motions may then be used as input to either total or effective stress site response codes to model nonlinear effects. Important issues associated with this approach include the availability of an appropriate nearby (1 to 2 km) rock outcrop and, for the downhole recordings, the necessity to remove all downgoing energy from the at-depth soil recordings. The downgoing energy must be removed from the downhole Green functions

[1]Kinematic source model is one whose slip (displacement) is defined (imposed) while in a dynamic source model forces (stress) are defined (see Aki and Richards 1980 for a complete description).

(recordings) prior to generating the control motions (summing) as only the upgoing wavefields are used as input to the nonlinear site response analyses. Removal of the downgoing energy from each recording requires multiple site response analyses which introduce uncertainty into the Green functions due to uncertainty in dynamic material properties and the numerical site response model used to separate the upgoing and downgoing wavefields.

To alleviate these difficulties one can use recordings well distributed in azimuth at close distances to a small earthquake and correct the recordings back to the source by removing wave propagation effects using a simple approximation (say 1/R plus a constant for crustal amplification and radiation pattern), to obtain an empirical source function. This source function can be used to replace the Brune pulse to introduce some natural (although source, path, and site specific) variation into the dislocation time history. If this is coupled to an approximate wave propagation algorithm (asymptotic ray theory) which includes the direct rays and those which have undergone a single reflection, the result is the empirical source function method (EPRI, 1993). Combining the reflectivity propagation (which is generally limited to frequencies $\leq$ 1-2 Hz due to computational demands) with the empirical source function approach (appropriate for frequencies $\geq$ 1 Hz; EPRI, 1993) results in a broad band simulation procedure which is strictly deterministic at low frequencies (where an analytical source function is used) and incorporates some natural variation at high frequencies through the use of an empirical source function (Sommerville et al., 1995).

All of these techniques are fundamentally similar, well founded in seismic source and wave propagation physics, and importantly, they are all approximate. Simply put, all models are wrong (approximate) and the single essential element in selecting a model is to incorporate the appropriate degree of rigor, commensurate with uncertainties and variabilities in crustal structure and site effects, through extensive validation exercises. It is generally felt that more complicated models produce more accurate results, however, the implications of more sophisticated models with the increased number of parameters which must be specified is often overlooked. This is not too serious a consequence in modeling past earthquakes since a reasonable range in parameter space can be explored to give the "best" results. However for future predictions, this increased rigor may carry undesirable baggage in increased parametric variability (Roblee et al., 1996). The effects of lack of knowledge (epistemic uncertainty; EPRI, 1993) regarding parameter values for future occurrences results in uncertainty or variability in ground motion predictions. It may easily be the case that a very simple model, such as the point-source model can have comparable, or even smaller, total variability (modeling plus parametric) than a much more rigorous model with an increased number of parameters (EPRI, 1993). What is desired in a model is sufficient sophistication such that it captures the dominant and stable features of source, distance, and site dependencies observed in strong ground motions. It is these considerations which led to the development of the stochastic point- and finite-source models and, in part, leads to the stochastic element of the models.

The stochastic nature of the point- and finite-source RVT models is simply the assumption made about the character of ground motion time histories that permits stable estimates of peak parameters (e.g. acceleration, velocity, strain, stress, oscillator response) to be made without computing detailed time histories (Hanks and McGuire, 1981; Boore, 1983). This process uses random vibration theory to relate a time domain peak value to the time history root-mean-square (RMS) value (Boore, 1983). The assumption of the character of the time history for this process to strictly apply is that it be normally distributed random noise and stationary (its statistics do not change with time) over its duration. A visual examination of any time history quickly reveals that this is clearly not the case: time histories (acceleration, velocity, stress, strain, oscillator) start, build up, and then diminish with time. However poor the assumption of stationary Gaussian noise may appear, the net result is that the assumption is weak enough to permit the approach to work surprisingly well, as numerous comparisons with recorded motions and both qualitative and quantative validations have shown (Hanks and McGuire, 1981; Boore, 1983, 1986; McGuire et al., 1984; Boore and Atkinson, 1987; Silva and Lee, 1987; Toro and McGuire, 1987; Silva et al., 1990; EPRI, 1993; Schneider et al., 1993; Silva and Darragh, 1995; Silva et al., 1997). Corrections to RVT are available to accommodate different distributions as well as non-

stationarity and are usually applied to the estimation of peak oscillator response in the calculated response spectra (Boore and Joyner, 1984; Toro, 1985).

Point-source Model

The conventional stochastic ground motion model uses an ω-square source model (Brune, 1970, 1971) with a single corner frequency and a constant stress drop (Boore, 1983; Atkinson, 1984). Random vibration theory is used to relate RMS (root-mean-square) values to peak values of acceleration (Boore, 1983), and oscillator response (Boore and Joyner, 1984; Toro, 1985; Silva and Lee, 1987) computed from the power spectra to expected peak time domain values (Boore, 1983).

The shape of the acceleration spectral density, a(f), is given by

$$a(f) = C \frac{f^2}{1+(\frac{f}{f_0})^2} \frac{MSUB0}{R} P(f) A(f) e^{-\frac{\pi f R}{\beta_0 Q(f)}} \qquad \text{(A-1)}$$

where

$$C = (\frac{1}{\rho_0 \beta_0^3}) \bullet (2) \bullet (0.55) \bullet (\frac{1}{\sqrt{2}}) \bullet \pi.$$

M_0 = seismic moment,
R = hypocentral distance,
β_0 = shear-wave velocity at the source,
ρ_0 = density at the source
Q(f) = frequency dependent quality factor (crustal damping),
A(f) = crustal amplification,
P(f) = high-frequency truncation filter,
f_o = source corner frequency.

C is a constant which contains source region density (ρ_0) and shear-wave velocity terms and accounts for the free-surface effect (factor of 2), the source radiation pattern averaged over a sphere (0.55) (Boore, 1986), and the partition of energy into two horizontal components ($1/\sqrt{2}$).

Source scaling is provided by specifying two independent parameters, the seismic moment (M_0) and the high-frequency stress parameter or stress drop ($\Delta\sigma$). The seismic moment is related to magnitude through the definition of moment magnitude **M** by the relation

$\log M_0 = 1.5\ \mathbf{M} + 16.05$ (Hanks and Kanamori, 1979) (A - 2).

The stress drop ($\Delta\sigma$) relates the corner frequency f_0 to M_0 through the relation

$f_0 = \beta_0 (\Delta\sigma/8.44\ M_0)^{1/3}$ (Brune; 1970, 1971) (A - 3).

The stress drop is sometimes referred to as the high frequency stress parameter (Boore, 1983) (or simply the stress parameter) since it directly scales the Fourier amplitude spectrum for frequencies above the corner frequency (Silva, 1991; Silva and Darragh 1995). High (> 1 Hz)

frequency model predictions are then very sensitive to this parameter (Silva, 1991; EPRI, 1993) and the interpretation of it being a stress drop or simply a scaling parameter depends upon how well real earthquake sources (on average) obey the omega-square scaling (Equation A-3) and how well they are fit by the single-corner-frequency model (Atkinson and Silva, 1997). If earthquakes truly have single-corner-frequency omega-square sources, the stress drop in Equation A-3 is a physical parameter and its values have a physical interpretation of the forces (stresses) accelerating the relative slip across the rupture surface. High stress drop sources are due to a smaller source (fault) area (for the same **M**) than low stress drop sources (Brune, 1970). Otherwise, it simply a high frequency ($f > f_o$) scaling or fitting parameter.

The spectral shape of the single-corner-frequency ω-square source model is then described by the two free parameters M_0 and $\Delta\sigma$. The corner frequency increases with the shear-wave velocity and with increasing stress drop, both of which may be region dependent.

The crustal amplification accounts for the increase in wave amplitude as seismic energy travels through lower- velocity crustal materials from the source to the surface. The amplification depends on average crustal and near surface shear-wave velocity and density (Boore, 1986).

The P(f) filter is used in an attempt to model the observation that acceleration spectral density appears to fall off rapidly beyond some region- or site-dependent maximum frequency (Hanks, 1982; Silva and Darragh, 1995). This observed phenomenon truncates the high frequency portion of the spectrum and is responsible for the band-limited nature of the stochastic model. The band limits are the source corner frequency at low frequency and the high frequency spectral attenuation. This spectral fall-off at high frequency has been attributed to near-site attenuation (Hanks, 1982; Anderson and Hough, 1984) or to source processes (Papageorgiou and Aki, 1983) or perhaps to both effects. In the Anderson and Hough (1984) attenuation model, adopted here, the form of the P(f) filter is taken as

$$P(f, r) = e^{-\pi\kappa(r)f} \qquad \text{(A-4)}.$$

Kappa (r) (κ(r) in Equation A-4) is a site and distance dependent parameter that represents the effect of intrinsic attenuation upon the wavefield as it propagates through the crust from source to receiver. Kappa (r) depends on epicentral distance (r) and on both the shear-wave velocity (β) and quality factor (Q_S) averaged over a depth of H beneath the site (Hough et al., 1988). At zero epicentral distance kappa (κ) is given by

$$\kappa(0) = \frac{H}{\bar{\beta}\,\bar{Q}_S} \qquad \text{(A-5)},$$

and is referred to as **K**.

The bar in Equation A-5 represents an average of these quantities over a depth H. The value of kappa at zero epicentral distance is attributed to attenuation in the very shallow crust directly below the site (Hough and Anderson, 1988; Silva and Darragh, 1995). The intrinsic attenuation along this part of the path is not thought to be frequency dependent and is modeled as a frequency independent, but site and crustal region dependent, constant value of kappa (Hough et al., 1988; Rovelli et al., 1988). This zero epicentral distance kappa is the model implemented in this study.

The crustal path attenuation from the source to just below the site is modeled with the frequency-dependent quality factor Q(f). Thus the distance component of the original **K**(r) (Equation A-4) is accommodated by Q(f) and R in the last term of Equation A-1:

$$\kappa(r) = \frac{H}{\overline{\beta}\,\overline{Q}_S} + \frac{R}{\beta_0\, Q(f)} \qquad \text{(A-6).}$$

The Fourier amplitude spectrum, a(f), given by Equation A-1 represents the stochastic ground motion model employing a Brune source spectrum that is characterized by a single corner frequency. It is a point source and models direct shear-waves in a homogeneous half-space (with effects of a velocity gradient captured by the A(f) filter, Equation A-1). For horizontal motions, vertically propagating shear-waves are assumed. Validations using incident inclined SH-waves accompanied with raytracing to find appropriate incidence angles leaving the source showed little reduction in uncertainty compared to results using vertically propagating shear-waves. For vertical motions, P/SV propagators are used coupled with raytracing to model incident inclined plane waves (EPRI, 1993). This approach has been validated with recordings from the 1989 **M** 6.9 Loma Prieta earthquake (EPRI, 1993).

Equation A-1 represents an elegant ground motion model that accommodates source and wave propagation physics as well as propagation path and site effects with an attractive simplicity. The model is appropriate for an engineering characterization of ground motion since it captures the general features of strong ground motion in terms of peak acceleration and spectral composition with a minimum of free parameters (Boore, 1983; McGuire et al., 1984; Boore, 1986; Silva and Green, 1988; Silva et al., 1988; Schneider et al., 1993; Silva and Darragh, 1995). An additional important aspect of the stochastic model employing a simple source description is that the region-dependent parameters may be evaluated by observations of small local or regional earthquakes. Region-specific seismic hazard evaluations can then be made for areas with sparse strong motion data with relatively simple spectral analyses of weak motion (Silva, 1992).

In order to compute peak time-domain values, i.e. peak acceleration and oscillator response, RVT is used to relate RMS computations to peak value estimates. Boore (1983) and Boore and Joyner (1984) present an excellent development of the RVT methodology as applied to the stochastic ground motion model. The procedure involves computing the RMS value by integrating the power spectrum from zero frequency to the Nyquist frequency and applying Parsevall's relation. Extreme value theory is then used to estimate the expected ratio of the peak value to the RMS value of a specified duration of the stochastic time history. The duration is taken as the inverse of the source corner frequency (Boore, 1983).

Factors that affect strong ground motions such as surface topography, finite and propagating seismic sources, laterally varying near-surface velocity and Q gradients, and random inhomogeneities along the propagation path are not included in the model. While some or all of these factors are generally present in any observation of ground motion and may exert controlling influences in some cases, the simple stochastic point-source model appears to be robust in predicting median or average properties of ground motion (Boore 1983, 1986; Schneider et al., 1993; Silva and Stark, 1993; Silva et al., 1997). The motivation for comprehensive validation exercises involving many earthquakes with a wide range in magnitudes, rupture distances, and site conditions is to capture unmodeled effects. The unmodeled effects which are random are captured in estimates of model uncertainty and those which are pervasive are captured in the estimates of model bias (see later sections). The combination of realistic, albeit simple, model physics with comprehensive validation exercises makes the stochastic point source ground motion model a powerful predictive and interpretative tool for engineering characterization of strong ground motion.

Finite-source Model Ground Motion Model

In the near-source region of large earthquakes, aspects of a finite-source including rupture propagation, directivity source-receiver geometry, and saturation of high-frequency (≥ 1 Hz) motions with increasing magnitude can be significant and may be incorporated into strong ground motion predictions. To accommodate these effects, a methodology that combines the aspects of finite-earthquake-source modeling techniques (Hartzell, 1978; Irikura 1983) with the stochastic

point-source ground motion model has been developed to produce response spectra as well as time histories appropriate for engineering design (Silva et al., 1990; Silva and Stark, 1993; Schneider et al., 1993). The approach is very similar to the empirical Green function methodology introduced by Hartzell (1978) and Irikura (1983). In this case however, the stochastic point-source is substituted for the empirical Green function and peak amplitudes; PGA, PGV, and response spectra (when time histories are not produced) are estimated using random process theory.

Use of the stochastic point-source as a Green function is motivated by its demonstrated success in modeling ground motions in general and strong ground motions in particular (Boore, 1983, 1986; Silva and Stark, 1993; Schneider et al., 1993; Silva and Darragh, 1995) and the desire to have a model that is truly site- and region-specific. The model can accommodate a region specific Q(f), Green function sources of arbitrary moment or stress drop, and site specific kappa values and soil profiles. The necessity for having available regional and site specific recordings distributed over the rupture surface of a future earthquake or modifying possibly inappropriate empirical Green functions is eliminated.

For the finite-source characterization, a rectangular fault is discretized into NS subfaults of moment M_0^S. The empirical relationship

$$\log (A) = \mathbf{M} - 4.0, \quad A \text{ in } km^2 \qquad \text{(A-7)}$$

is used to assign areas to both the target earthquake (if its rupture surface is not fixed) as well as to the subfaults. This relation results from regressing log area on **M** using the data of Wells and Coppersmith (1994). In the regression, the coefficient on **M** is set to unity which implies a constant static stress drop of about 30 bars (Equation A-9). This is consistent with the general observation of a constant static stress drop for earthquakes based on aftershock locations (Wells and Coppersmith 1994). The static stress drop, defined by Equation A-10, is related to the average slip over the rupture surface as well as rupture area. It is theoretically identical to the stress drop in Equation A-3 which defines the omega-square source corner frequency assuming the rupture surface is a circular crack model (Brune, 1970; 1971). The stress drop determined by the source corner frequency (or source duration) is usually estimated through the Fourier amplitude spectral density while the static stress drop uses the moment magnitude and an estimate of the rupture area. The two estimates for the same earthquake seldom yield the same values with the static generally being the smaller. In a recent study (Silva et al., 1997), the average stress drop based on Fourier amplitude spectra determined from an empirical attenuation relation (Abrahamson and Silva, 1997) is about 70 bars while the average static stress drop for the crustal earthquakes studied by Wells and Coppersmith (1994) is about 30 bars. These results reflect a general factor of about 2 on average between the two values. These large differences may simply be the result of using an inappropriate estimate of rupture area as the zone of actual slip is difficult to determine unambiguously. In general however, even for individual earthquakes, the two stress drops scale similarly with high static stress drops (> 30 bars) resulting in large high frequency (> 1 Hz for $\mathbf{M} \geq 5$) ground motions which translates to high corner frequencies (Equation A-3).

The subevent magnitude M_S is generally taken in the range of 5.0-6.5 depending upon the size of the target event. M_S 5.0 is used for crustal earthquakes with **M** in the range of 5.5 to 8.0 and M_S 6.4 is used for large subduction earthquakes with **M** > 7.5. The value of NS is determined as the ratio of the target event area to the subfault area. To constrain the proper moment, the total number of events summed (N) is given by the ratio of the target event moment to the subevent moment. The subevent and target event rise times (duration of slip at a point) are determined by the equation

$$\log \mathbf{T} = 0.33 \log M_0 - 8.54 \qquad \text{(A-8)}$$

which results from a fit to the rise times used in the finite-fault modeling exercises, (Silva et al., 1997). Slip on each subfault is assumed to continue for a time **T**. The ratio of target-to-subevent rise times is given by

$$\frac{\tau}{\tau^s} = 10^{0.5\,(\mathrm{M}\,-\,\mathrm{MSUPs})} \qquad \text{(A-9)}$$

and determines the number of subevents to sum in each subfault. This approach is generally referred to as the constant-rise-time model and results in variable slip velocity for nonuniform slip distributions. Alternatively, one can assume a constant slip velocity (as do Beresnev and Atkinson, 2002) resulting in a variable-rise-time model for heterogenous slip distributions. This approach was implemented and validations resulted in an overall "best" average slip velocity of about 70 cm/sec, with no significant improvement over a magnitude dependent rise time (Equation A-8). The feature is retained as an option in the simulation code.

Recent modeling of the Landers (Wald and Heaton, 1994), Kobe (Wald, 1996) and Northridge (Hartzell et al. 1996) earthquakes suggests that a mixture of both constant rise time and constant slip velocity may be present. Longer rise times seem to be associated with areas of larger slip with the ratio of slip-to-rise time (slip velocity) being depth dependent. Lower slip velocities (longer rise times) are associated with shallow slip resulting in relatively less short period seismic radiation. This result may explain the general observation that shallow slip is largely aseismic. The significant contributions to strong ground motions appear to originate at depths exceeding about 4 km (Campbell, 1993; Boore et al., 1994) as the fictitious depth term in empirical attenuation relation (Abrahamson and Silva, 1997; Boore et al., 1997). Finite-fault models generally predict unrealistically large strong ground motions for large shallow (near surface) slip using rise times or slip velocities associated with deeper (> 4 km) zones of slip. This is an important and unresolved issue in finite-fault modeling and the general approach is constrain the slip to relatively small values in the top 2 to 4 km. For the composite source model, the approach is to taper the subevent stress drop to zero at the ground surface (Yehua Zeng, personal communication 1999). A more thorough analysis is necessary, ideally using several well validated models, before this issue can be satisfactorily resolved.

To introduce heterogeneity of the earthquake source process into the stochastic finite-fault model, the location of the sub-events within each subfault (Hartzell, 1978) are randomized as well as the subevent rise time (σ_{ln} = 0.8). The stress drop of the stochastic point-source Green function is taken as 30 bars, consistent with the static value based on the **M** 5.0 subevent area using the equation

$$\Delta\sigma = \frac{7}{16}\left(\frac{M_e}{R_e^3}\right) \qquad \text{(Brune, 1970, 1971)} \qquad \text{(A-10)}$$

where R_e is the equivalent circular radius of the rectangular sub-event.

Different values of slip are assigned to each subfault as relative weights so that asperities or non-uniform slip can be incorporated into the methodology. For validation exercises, slip models are taken from the literature and are based on inversions of strong motion as well as regional or teleseismic recordings. To produce slip distributions for future earthquakes, random slip models are generated based on a statistical asperity model with parameters calibrated to the published slip distributions. This approach has been validated by comparing the modeling uncertainty and bias estimates for the Loma Prieta and Whittier Narrows earthquakes using motion at each site averaged over several (30) random slip models to the bias and uncertainty estimates using the published slip model. The results show nearly identical bias and uncertainty estimates

suggesting that averaging the motions over random slip models produces as accurate a prediction at a site as a single motion computed using the "true" slip model which is determined from inverting actual recordings.

The rupture velocity is taken as depth independent at a value of 0.8 times the shear-wave velocity, generally at the depth of the dominant slip. This value is based on a number of studies of source rupture processes which also suggest that rupture velocity is non-uniform. To capture the effects of non-uniform rupture velocity, a random component is added through the randomized location of the subevents within each subfault. The radiation pattern is computed for each subfault, a random component added, and the RMS applied to the motions computed at the site when modeling an average horizontal component. To model individual horizontal components, the radiation pattern for each subfault is used to scale each subfaults contribution to the final summed motion.

The ground-motion time history at the receiver is computed by summing the contributions from each subfault associated with the closest Green function, transforming to the frequency domain, and convolving with the appropriate Green function spectrum (Equation A-1). The locations of the Green functions are generally taken at center of each subfault for small subfaults or at a maximum separation of about 5 to 10 km for large subfaults. As a final step, the individual contributions associated with each Green function are summed in the frequency domain, multiplied by the RMS radiation pattern, and the resultant power spectrum at the site is computed. The appropriate duration used in the RVT computations for PGA, PGV, and oscillator response is computed by transforming the summed Fourier spectrum into the time domain and computing the 5 to 75% Arias intensity (Ou and Herrmann, 1990).

As with the point-source model, crustal response effects are accommodated through the amplification factor (A(f)) or by using vertically propagating shear waves through a vertically heterogenous crustal structure. Propagation path damping, through the Q(f) model, is incorporated from each fault element to the site. Near-surface crustal damping is incorporated through the kappa operator (Equation A-1). To model crustal propagation path effects, the raytracing method of Ou and Herrmann (1990) is applied from each subfault to the site.

Time histories may be computed in the process as well by simply adding a phase spectrum appropriate to the subevent earthquake. The phase spectrum can be extracted from a recording made at close distance to an earthquake of a size comparable to that of the subevent (generally **M** 5.0 to 6.5). Interestingly, the phase spectrum need not be from a recording in the region of interest (Silva et al., 1989). A recording in WNA (Western North America) can effectively be used to simulate motions appropriate to ENA (Eastern North America). Transforming the Fourier spectrum computed at the site into the time domain results in a computed time history which then includes all of the aspects of rupture propagation and source finiteness, as well as region specific propagation path and site effects.

For fixed fault size, mechanism, and moment, the specific source parameters for the finite-fault are slip distribution, location of nucleation point, and site azimuth. The propagation path and site parameters remain identical for both the point- and finite-source models.

Partition and assessment of ground motion variability

An essential requirement of any numerical modeling approach, particularly one which is implemented in the process of defining design ground motions, is a quantative assessment of prediction accuracy. A desirable approach to achieving this goal is in a manner which lends itself to characterizing the variability associated with model predictions. For a ground motion model, prediction variability is comprised of two components: modeling variability and parametric variability. Modeling variability is a measure of how well the model works (how accurately it predicts ground motions) when specific parameter values are known. Modeling variability is measured by misfits of model predictions to recorded motions through validation exercises and is due to unaccounted for components in the source, path, and site models (i.e. a point-source

cannot model the effects of directivity and linear site response cannot accommodate nonlinear effects). Results from a viable range of values for model parameters (i.e., slip distribution, soil profile, G/G_{max} and hysteretic damping curves, etc). Parametric variability is the sensitivity of a model to a viable range of values for model parameters. The total variability, modeling plus parametric, represents the variance associated with the ground motion prediction and, because it is a necessary component in estimating fractile levels, may be regarded as important as median predictions.

Both the modeling and parametric variabilities may have components of randomness and uncertainty. Table A.1 summarizes the four components of total variability in the context of ground motion predictions. Uncertainty is that portion of both modeling and parametric variability which, in principle, can be reduced as additional information becomes available, whereas randomness represents the intrinsic or irreducible component of variability for a given model or parameter. Randomness is that component of variability which is intrinsic or irreducible for a given model. The uncertainty component reflects a lack of knowledge and may be reduced as more data are analyzed. For example, in the point-source model, stress drop is generally taken to be independent of source mechanism as well as tectonic region and is found to have a standard error of about 0.7 (natural log) for the CEUS (EPRI, 1993). This variation or uncertainty plus randomness in $\Delta\sigma$ results in a variability in ground motion predictions for future earthquakes. If, for example, it is found that normal faulting earthquakes have generally lower stress drops than strike-slip which are, in turn, lower than reverse mechanism earthquakes, perhaps much of the variability in $\Delta\sigma$ may be reduced. In extensional regimes, where normal faulting earthquakes are most likely to occur, this new information may provide a reduction in variability (uncertainty component) for stress drop, say to 0.3 or 0.4 resulting in less ground motion variation due to a lack of knowledge of the mean or median stress drop. There is, however, a component of this stress drop variability which can never be reduced in the context of the Brune model. This is simply due to the heterogeneity of the earthquake dynamics which is not accounted for in the model and results in the randomness component of parametric variability in stress drop. A more sophisticated model may be able to accommodate or model more accurately source dynamics but, perhaps, at the expense of a larger number of parameters and increased parametric uncertainty (i.e. the finite-fault with slip model and nucleation point as unknown parameters for future earthquakes). That is, more complex models typically seek to reduce modeling randomness by more closely modeling physical phenomena. However, such models often require more comprehensive sets of observed data to constrain additional model parameters, which generally leads to increased parametric variability. If the increased parametric variability is primarily in the form of uncertainty, it is possible to reduce total variability, but only at the additional expense of constraining the additional parameters. Therefore, existing knowledge and/or available resources may limit the ability of more complex models to reduce total variability.

The distinction of randomness and uncertainty is model driven and somewhat arbitrary. The allocation is only important in the context of probabilistic seismic hazard analyses as uncertainty is treated as alternative hypotheses in logic trees while randomness is integrated over in the hazard calculation (Cornell, 1968). For example, the uncertainty component in stress drop may be treated by using an N-point approximation to the stress drop distribution and assigning a branch in a logic tree for each stress drop and associated weight. A reasonable three point approximation to a normal distribution is given by weights of 0.2, 0.6, 0.2 for expected 5%, mean, and 95% values of stress drop respectively. If the distribution of uncertainty in stress drop was such that the 5%, mean, and 95% values were 50, 100, and 200 bars respectively, the stress drop branch on a logic tree would have 50, and 200 bars with weights of 0.2 and 100 bars with a weight of 0.6. The randomness component in stress drop variability would then be formally integrated over in the hazard calculation.

Assessment of Modeling Variability

Modeling variability (uncertainty plus randomness) is usually evaluated by comparing response spectra computed from recordings to predicted spectra and is a direct assessment of model

accuracy. The modeling variability is defined as the standard error of the residuals of the log of the average horizontal component (or vertical component) response spectra. The residual is defined as the difference of the logarithms of the observed average 5% damped acceleration response spectra and the predicted response spectra. At each period, the residuals are squared, and summed over the total number of sites for one or all earthquakes modeled. Dividing the resultant sum by the number of sites results in an estimate of the model variance. Any model bias (average offset) that exists may be estimated in the process (Abrahamson et al., 1990; EPRI, 1993) and used to correct (lower) the variance (and to adjust the median as well). In this approach, the modeling variability can be separated into randomness and uncertainty where the bias corrected variability represents randomness and the total variability represents randomness plus uncertainty. The uncertainty is captured in the model bias as this may be reduced in the future by refining the model. The remaining variability (randomness) remains irreducible for this model. In computing the variance and bias estimates only the frequency range between processing filters at each site (minimum of the 2 components) should be used.

Assessment of Parametric Variability

Parametric variability, or the variation in ground motion predictions due to uncertainty and randomness in model parameters is difficult to assess. Formally, it is straight-forward in that a Monte Carlo approach may be used with each parameter randomly sampled about its mean (median) value either individually for sensitivity analyses (Silva, 1992; Roblee et al., 1996) or in combination to estimate the total parametric variability (Silva, 1992; EPRI, 1993). In reality, however, there are two complicating factors.

The first factor involves the specific parameters kept fixed with all earthquakes, paths, and sites when computing the modeling variability. These parameters are then implicitly included in modeling variability provided the data sample a sufficiently wide range in source, path, and site conditions. The parameters which are varied during the assessment of modeling variation should have a degree of uncertainty and randomness associated with them for the next earthquake. Any ground motion prediction should then have a variation reflecting this lack of knowledge and randomness in the free parameters.

An important adjunct to fixed and free parameters is the issue of parameters which may vary but by fixed rules. For example, source rise time (Equation A-8) is magnitude dependent and in the stochastic finite-source model is specified by an empirical relation. In evaluating the modeling variability with different magnitude earthquakes, rise time is varied, but because it follows a strict rule, any variability associated with rise time variation is counted in modeling variability. This is strictly true only if the sample of earthquakes has adequately spanned the space of magnitude, source mechanism, and other factors which may affect rise time. Also, the earthquake to be modeled must be within that validation space. As a result, the validation or assessment of model variation should be done on as large a number of earthquakes of varying sizes and mechanisms as possible.

The second, more obvious factor in assessing parametric variability is a knowledge of the appropriate distributions for the parameters (assuming correct values for median or mean estimates are known). In general, for the stochastic models, median parameter values and uncertainties are based, to the extent possible, on evaluating the parameters derived from previous earthquakes (Silva, 1992; EPRI, 1993).

The parametric variability is site, path, and source dependent and must be evaluated for each modeling application (Roblee et al., 1996). For example, at large source-to-site distances, crustal path damping may control short-period motions. At close distances to a large fault, both the site and finite-source (asperity location and nucleation point) may dominate, and, depending upon site characteristics, the source or site may control different frequency ranges (Silva, 1992; Roblee et al., 1996). Additionally, level of control motion may affect the relative importance of G/G_{max} and hysteretic damping curves.

In combining modeling and parametric variations, independence is assumed (covariance is zero) and the variances are simply added to give the total variability.

$$_{ln}\sigma^2_T = {}_{ln}\sigma^2_{\mathbf{M}} + {}_{ln}\sigma^2_P{}^2 \qquad \text{(A-11)},$$

where

$_{ln}\sigma^2_{\mathbf{M}}$ = modeling variation,

$_{ln}\sigma^2_P$ = parametric variation.

Validation Of The Point- and Finite-Source Models

In a recent Department of Energy sponsored project (Silva et al., 1997), both the point- and finite-source stochastic models were validated in a systematic and comprehensive manner. In this project, 16 well recorded earthquakes were modeled at about 500 sites. Magnitudes ranged from **M** 5.3 to **M** 7.4 with fault distances from about 1 km out to 218 km for WUS earthquakes and 460 km for CEUS earthquakes. This range in magnitude and distance as well as number of earthquakes and sites results in the most comprehensively validated model currently available to simulate strong ground motions.

For these exercises, regional Q(f) models and point source stress drops were determined through inversions using the strong motion recordings (Silva et al., 1997). Small strain WUS rock and soil kappa values were set to 0.04 sec, the average from the inversions of small strain data. CEUS rock site kappa values were fixed at inversion values, which averaged about 0.02 sec and ranged from 0.004 to 0.06 sec. For the finite source parameters, slip models and nucleation points were taken from the literature (Silva et al., 1997). Point-source depths were taken as the depth of the center of the largest asperity in the slip models while point-source distance used the closest distance to the surface projection of the rupture surface.

A unique aspect of this validation is that rock and soil sites were modeled using generic rock and soil profiles and equivalent-linear site response. Validations done with other simulation procedures typically neglect site conditions as well as nonlinearity resulting in ambiguity in interpretation of the simulated motions.

Point-Source Model

Final model bias and variability estimates for the point-source model are shown in Figure A1. Over all the sites (Figure A1) the bias is slightly positive for frequencies greater than about 10 Hz and is near zero from about 10 Hz to 1 Hz. Below 1 Hz, a stable point-source overprediction is reflected in the negative bias. The analyses are considered reliable down to about 0.3 Hz (3.3 sec) where the point-source shows about a 40% overprediction.

The model variability is low, about 0.5 above about 3 to 4 Hz and increases with decreasing frequency to near 1 at 0.3 Hz. Above 1 Hz, there is little difference between the total variability (uncertainty plus randomness) and randomness (bias corrected variability) reflecting the near zero bias estimates. Below 1 Hz there is considerable uncertainty contributing to the total variability suggesting that the model can be measurably improved as its predictions tend to be

[2]Strong ground motions are generally considered to be log normally distributed.

consistently high at very low frequencies ($\leq$ 1 Hz). This stable misfit may be interpreted as the presence of a second corner frequency for WNA sources (Atkinson and Silva, 1997).

Finite-Source Model

For the finite-fault, Figure A2 shows the corresponding bias and variability estimates. For all the sites, the finite-source model provides slightly smaller bias estimates and, surprisingly, slightly higher variability for frequencies exceeding about 5 Hz. The low frequency ($\leq$ 1 Hz) point-source overprediction is not present in the finite-source results, indicating that it is giving more accurate predictions than the point-source model over a broad frequency range, from about 0.3 Hz (the lowest frequency of reliable analyses) to the highest frequency of the analyses.

In general, for frequencies of about 1 Hz and above the point-source and finite-source give comparable results: the bias estimates are small (near zero) and the variabilities range from about 0.5 to 0.6. These estimates are low considering the analyses are based on a data set comprised of earthquakes with **M** less than **M** 6.5 (288 of 513 sites) and high frequency ground motion variance decreases with increasing magnitude, particularly above **M** 6.5 (Youngs et al., 1995) Additionally, for the vast majority of sites, generic site conditions were used (inversion kappa values were used for only the Saguenay and Nahanni earthquake analyses, 25 rock sites). As a result, the model variability (mean = 0) contains the total uncertainty and randomness contribution for the site. The parametric variability due to uncertainty and randomness in site parameters: shear-wave velocity, profile depth, G/G_{max} and hysteretic damping curves need not be added to the model variability estimates. It is useful to perform parametric variations to assess site parameter sensitivities on the ground motions, but only source and path damping Q(f) parametric variabilities require assessment on a site specific basis and added to the model variability. The source uncertainty and randomness components include point-source stress drop as well as source depth and finite-source slip model and nucleation point (Silva, 1992).

The general approach taken in these validations is to have few free parameters and accept a relatively large model misfit. This approach relaxes the need to develop appropriate distributions for poorly resolved parameters such as spatially varying rise times and rupture velocity as well as non-planar rupture surfaces (e.g. Landers, Kobe, and Kocaeli earthquakes). An alternative approach is to adjust these suites of parameters, which naturally improves the fits to recorded motions and results in smaller modeling uncertainties. However, unless independent information is available to constrain these parameters for future earthquakes, they must be appropriately counted as parametric variability. This may result in the total variability remaining comparable between the two approaches. This concept parallels the utility of increased model complexity, i.e., simple verses complex models. More complex models may increase an understanding of physical processes but, in the context of predicting motions due to the next earthquake, increased model complexity may not provide more accurate estimates of strong ground motions, again unless independent information is available to constrain potential ranges in some or all of the free parameters.

A summary of fixed and free parameters for the implementation of the stochastic point and finite source models presented here is listed in Table 2.

Empirical Attenuation Model

As an additional assessment of the stochastic models, bias and variability estimates were made over the same earthquakes (except Saguenay since it was not used in the regressions) and sites using a recently develop empirical attenuation relation (Abrahamson and Silva, 1997). For all the sites, the estimates are shown in Figure A3. Interestingly, the point-source overprediction below about 1 Hz is present in the empirical relation perhaps suggesting that this suite of earthquakes possess lower than expected motions in this frequency range as the empirical model does not show this bias over all earthquakes ($\approx$ 50) used in its development. Comparing these results to the point- and finite-source results (Figures A1 and A2) show comparable bias and variability estimates. For future predictions, source and path damping parametric variability must be added

to the numerical simulations which will contribute a σ_{ln} of about 0.2 to 0.4, depending upon frequency, source and path conditions, and site location. This will raise the modeling variability from about 0.50 to the range of 0.54 to 0.64, about 10 to 30%. These values are still comparable to the variability of the empirical relation indicating that the point- and finite-source numerical models perform about as well as a recently developed empirical attenuation relation for the validation earthquakes and sites.

These results are very encouraging and provide an additional qualitative validation of the point- and finite-source models. Paranthetically this approach provides a rational basis for evaluating empirical attenuation models.

APPENDIX A

REFERENCES

Abrahamson, N.A. and W.J. Silva (1997). "Empirical response spectral attenuation relations for shallow crustal earthquakes." *Seismological Research Let.,* 68(1), 94-127.

Abrahamson, N.A., P.G. Somerville, and C.A. Cornell (1990). "Uncertainty in numerical strong motion predictions" *Proc. Fourth U.S. Nat. Conf. Earth. Engin.*, Palm Springs, CA., 1, 407-416.

Aki, K. and P.G. Richards. (1980). *"Quantitative siesmology."* W. H. Freeman and Co., San Francisco, California.

Atkinson, G.M and W.J. Silva (1997). "An empirical study of earthquake source spectra for California earthquakes." *Bull. Seism. Soc. Am.* 87(1), 97-113.

Anderson, J.G. and S.E. Hough (1984). "A Model for the Shape of the Fourier Amplitude Spectrum of Acceleration at High Frequencies." *Bulletin of the Seismological Society of America,* 74(5), 1969-1993.

Atkinson, G.M. (1984). "Attenuation of strong ground motion in Canada from a random vibrations approach." *Bull. Seism. Soc. Am.*, 74(5), 2629-2653.

Beresnev, I.A. and G. M. Atkinson (2002). "Source parameters of earthquakes in Eastern and Western North America." *Bull. Seism. Soc. Am.,* 92(2), 695-710.

Boore, D.M., W.B. Joyner, and T.E. Fumal (1997). "Equations for estimating horizontal response spectra and peak acceleration from Western North American earthquakes: A summary of recent work." *Seism. Res. Lett.* 68(1), 128-153.

Boore, D.M., W.B. Joyner, and T.E. Fumal (1994). "Estimation of response spectra and peak accelerations from western North American earthquakes: and interim report. Part 2. *U.S. Geological Survey Open-File Rept.* 94-127.

Boore, D.M., and G.M. Atkinson (1987). "Stochastic prediction of ground motion and spectral response parameters at hard-rock sites in eastern North America." *Bull. Seism. Soc. Am.*, 77(2), 440-467.

Boore, D.M. (1986). "Short-period P- and S-wave radiation from large earthquakes: implications for spectral scaling relations." *Bull. Seism. Soc. Am.*, 76(1) 43-64.

Boore, D.M. and W.B. Joyner (1984). "A note on the use of random vibration theory to predict peak amplitudes of transient signals." *Bull. Seism. Soc. Am.*, 74, 2035-2039.

Boore, D.M. (1983). "Stochastic simulation of high-frequency ground motions based on seismological models of the radiated spectra." *Bull. Seism. Soc. Am.*, 73(6), 1865-1894.

Brune, J.N. (1971). "Correction." *J. Geophys. Res.* 76, 5002.

Brune, J.N. (1970). "Tectonic stress and the spectra of seismic shear waves from earthquakes." *J. Geophys. Res.* 75, 4997-5009.

Campbell, K.W. (1993) "Empirical prediction of near-source ground motion from large earthquakes." in V.K. Gaur, ed., *Proceedings, Intern'l Workshop on Earthquake Hazard and Large Dams in the Himalya.* INTACH, New Delhi, p. 93-103.

Cornell, C.A. (1968). "Engineering seismic risk analysis." *Bull. Seism. Soc. Am.*, 58, 1583-1606.

Electric Power Research Institute (1993). "Guidelines for determining design basis ground motions." Palo Alto, Calif: Electric Power Research Institute, vol. 1-5, EPRI TR-102293.
vol. 1: Methodology and guidelines for estimating earthquake ground motion in eastern North America.
vol. 2: Appendices for ground motion estimation.
vol. 3: Appendices for field investigations.
vol. 4: Appendices for laboratory investigations.
vol. 5: Quantification of seismic source effects.

Hanks, T.C. (1982). "f_{max}." *Bull. Seism. Soc. Am.,* 72, 1867-1879.

Hanks, T.C. and R.K. McGuire (1981). "The character of high-frequency strong ground motion." *Bull. Seism. Soc. Am.*, 71(6), 2071-2095.

Hanks, T.C. and H. Kanamori (1979). "A moment magnitude scale." *J. Geophys. Res.*, 84, 2348-2350.

Hartzell, S., A. Leeds, A. Frankel, and J. Michael (1996). "Site response for urban Los Angeles using aftershocks of the Northridge earthquake." *Bull. Seism. Soc. Am.*, 86(1B), S168-S192.

Hartzell, S.H. (1978). "Earthquake aftershocks as Green's functions." *Geophys. Res. Letters*, 5, 1-4.

Hough, S.E., J.G. Anderson, J. Brune, F. Vernon III, J. Berger, J. Fletcher, L. Haar, T. Hanks, and L. Baker (1988). "Attenuation near Anza, California." *Bull. Seism. Soc. Am.*, 78(2), 672-691.

Hough, S.E. and J.G. Anderson (1988). "High-Frequency Spectra Observed at Anza, California: Implications for Q Structure." *Bull. Seism. Soc. Am.*, 78(2), 692-707.

Irikura, K. (1983). "Semi-empirical estimation of strong ground motions during large earthquakes." *Bull. Disaster Prevention Res. Inst.*, Kyoto Univ., 33, 63-104.

McGuire, R. K., A.M. Becker, and N.C. Donovan (1984). "Spectral Estimates of Seismic Shear Waves." *Bull. Seism. Soc. Am.*, 74(4), 1427-1440.

Ou, G.B. and R.B. Herrmann (1990). "Estimation theory for strong ground motion." *Seism. Res. Letters.* 61.

Papageorgiou, A.S. and K. Aki (1983). "A specific barrier model for the quantitative description of inhomogeneous faulting and the prediction of strong ground motion, part I, Description of the model." *Bull. Seism. Soc. Am.*, 73(4), 693-722.

Roblee, C.J., W.J. Silva, G.R. Toro and N. Abrahamson (1996). "Variability in site-specific seismic ground-motion design predictions." in press.

Rovelli, A., O. Bonamassa, M. Cocco, M. Di Bona, and S. Mazza (1988). "Scaling laws and spectral parameters of the ground motion in active extensional areas in Italy." *Bull. Seism. Soc. Am.*, 78(2), 530-560.

Schneider, J.F., W.J. Silva, and C.L. Stark (1993). "Ground motion model for the 1989 **M** 6.9 Loma Prieta earthquake including effects of source, path and site." *Earthquake Spectra*, 9(2), 251-287.

Silva, W.J., N. Abrahamson, G. Toro, and C. Costantino (1997). "Description and validation of the stochastic ground motion model." Submitted to Brookhaven National Laboratory, Associated Universities, Inc. Upton, New York.

Silva, W.J. and R. Darragh (1995). "Engineering characterization of earthquake strong ground motion recorded at rock sites." Palo Alto, Calif:Electric Power Research Institute, TR-102261.

Silva, W.J. and C.L. Stark (1993) "Source, path, and site ground motion model for the 1989 **M** 6.9 Loma Prieta earthquake." CDMG draft final report.

Silva, W.J. (1992). "Factors controlling strong ground motions and their associated uncertainties." *Dynamic Analysis and Design Considerations for High Level Nuclear Waste Repositories, ASCE* 132-161.

Silva, W.J. (1991). "Global characteristics and site geometry." Chapter 6 in *Proceedings: NSF/EPRI Workshop on Dynamic Soil Properties and Site Characterization.* Palo Alto, Calif.: Electric Power Research Institute, NP-7337.

Silva, W. J., R. Darragh, C. Stark, I. Wong, J. C. Stepp, J. Schneider, and S-J. Chiou (1990). "A Methodology to Estimate Design Response Spectra in the Near-Source Region of Large Earthquakes Using the Band-Limited-White-Noise Ground Motion Model". *Procee. of the Fourth U.S. Conf. on Earthquake Engineering,* Palm Springs, California. 1, 487-494.

Silva, W.J., R.B. Darragh, R.K. Green and F.T. Turcotte (1989). *Estimated Ground Motions for a new madrid Event.* U.S. Army Engineer Waterways Experiment Station, Wash., DC, Misc. Paper GL-89-17.

Silva, W. J. and R. K. Green (1988). "Magnitude and Distance Scaling of Response Spectral Shapes for Rock Sites with Applications to North American Environments." In *Proceedings: Workshop on Estimation of Ground Motion in the Eastern United States*, EPRI NP-5875, Electric Power Research Institute.

Silva, W. J., T. Turcotte, and Y. Moriwaki (1988). "Soil Response to Earthquake Ground Motion," Electric Power Research Institute, Walnut Creek, California, Report No. NP-5747.

Silva, W.J. and K. Lee (1987). "*WES RASCAL code for synthesizing earthquake ground motions.*" State-of-the-Art for Assessing Earthquake Hazards in the United States, Report 24, U.S. Army Engineers Waterways Experiment Station, Miscellaneous Paper S-73-1.

Somerville, P.G., R. Graves and C. Saikia (1995). "TECHNICAL REPORT: Characterization of ground motions during the Northridge earthquake of January 17, 1994." *Structural Engineers Association of California (SEAOC).* Report No. SAC-95-03.

Toro, G. R. and R. K. McGuire (1987). "An Investigation into Earthquake Ground Motion Characteristics in Eastern North America." *Bull. Seism. Soc. Am.*, 77(2), 468-489.

Toro, G. R. (1985). "Stochastic Model Estimates of Strong Ground Motion." In *Seismic Hazard Methodology for Nuclear Facilities in the Eastern United States*, Appendix B, R. K. McGuire, ed., Electric Power Research Institute, Project P101-29.

Wald, D.J. (1996). "Slip history of the 1995 Kobe, Japan, earthquake determined from strong motion, teleseismic, and geodetic data." *J. of Physics of the Earth,* in press.

Wald, D.J. and T.H. Heaton (1994). "Spatial and temporal distribution of slip for the 1992 Landers, California, earthquake." *Bull. Seism. Soc. Amer.*, 84(3), 668-691.

Wells, D.L. and K.J. Coppersmith (1994). "New empirical relationships among magnitude, rupture length, rupture width, rupture area, and surface displacement." *Bull. Seism. Soc. Am.* 84(4), 974-1002.

Youngs, R.R., N.A. Abrahamson, F. Makdisi, and K. Sadigh (1995). "Magnitude dependent

dispersion in peak ground acceleration." *Bull. Seism. Soc. Amer.*, 85(1), 161-1, 176.

Table A.1

CONTRIBUTIONS TO TOTAL VARIABILITY
IN GROUND MOTION MODELS

	Modeling Variability	Parametric Variability
Uncertainty *(also Epistemic Uncertainty)*	Modeling Uncertainty: Variability in predicted motions resulting from particular model assumptions, simplifications and/or fixed parameter values. *Can be reduced by adjusting or "calibrating" model to better fit observed earthquake response.*	Parametric Uncertainty: Variability in predicted motions resulting from incomplete data needed to characterize parameters. *Can be reduced by collection of additional information which better constrains parameters*
Randomness *(also Aleatory Uncertainty)*	Modeling Randomness: Variability in predicted motions resulting from discrepancies between model and actual complex physical processes. *Cannot be reduced for a given model form.*	Parametric Randomness: Variability in predicted motions resulting from inherent randomness of parameter values. *Cannot be reduced a priori*[***] *by collection of additional information.*

[***]Some parameters (e.g. source characteristics) may be well defined after an earthquakes.

Table A.2

FIXED AND FREE PARAMETERS

Fixed Parameters

- Regional Curstal Model
- Rock and Soil Generic Profiles
- Kappa
- G/Gmax and Hysteric Damping Curves
- Finite Source Rise Time
- Finite Source Rupture Velocity

Free Parameters

- Regional Q(f) Model
- Point Source Stress Drop and Depth
- Finite Source Slip Model and Nucleation Point

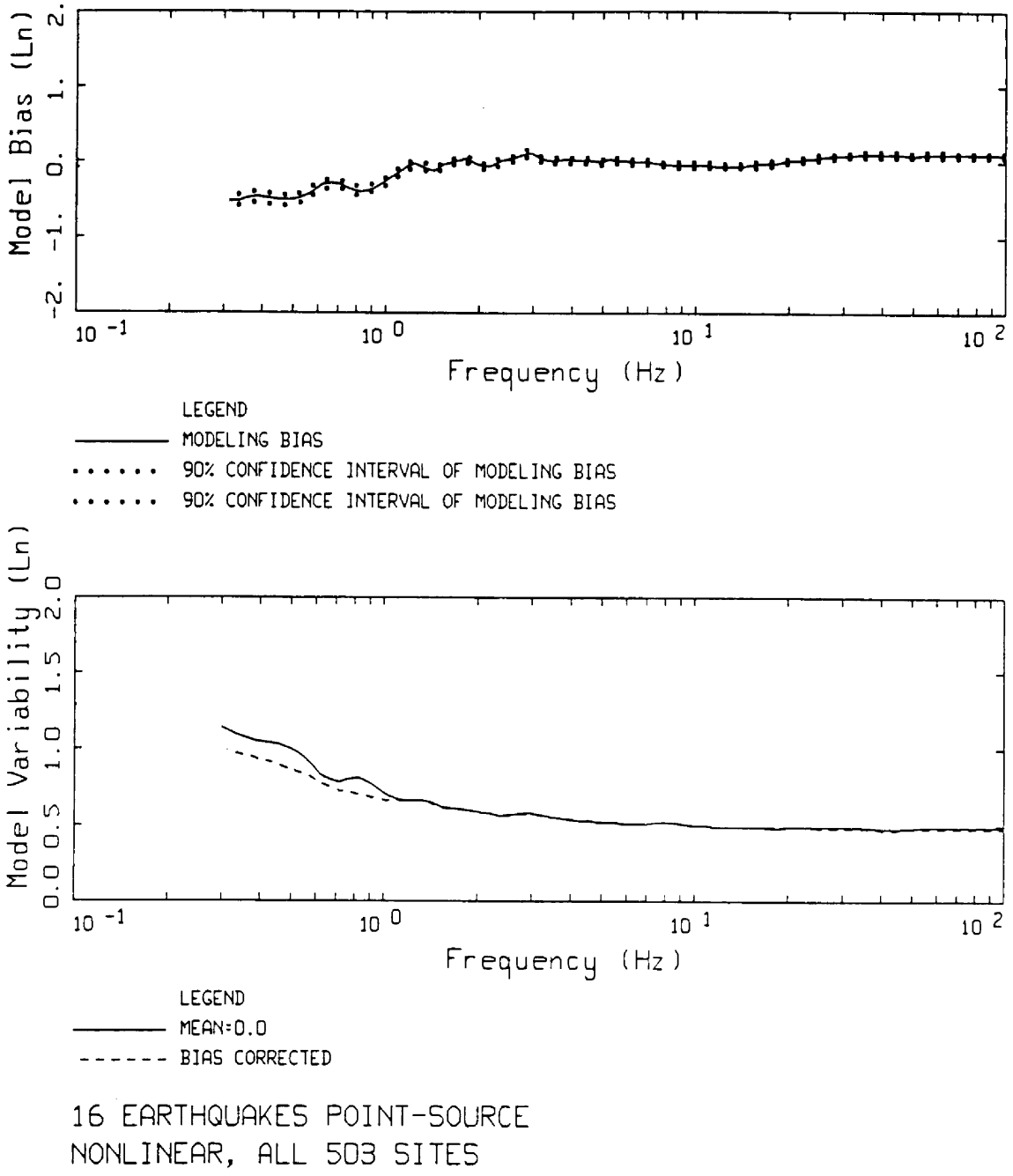

Figure A1. Model bias and variability estimates for all earthquakes computed over all 503 sites for the point-source model.

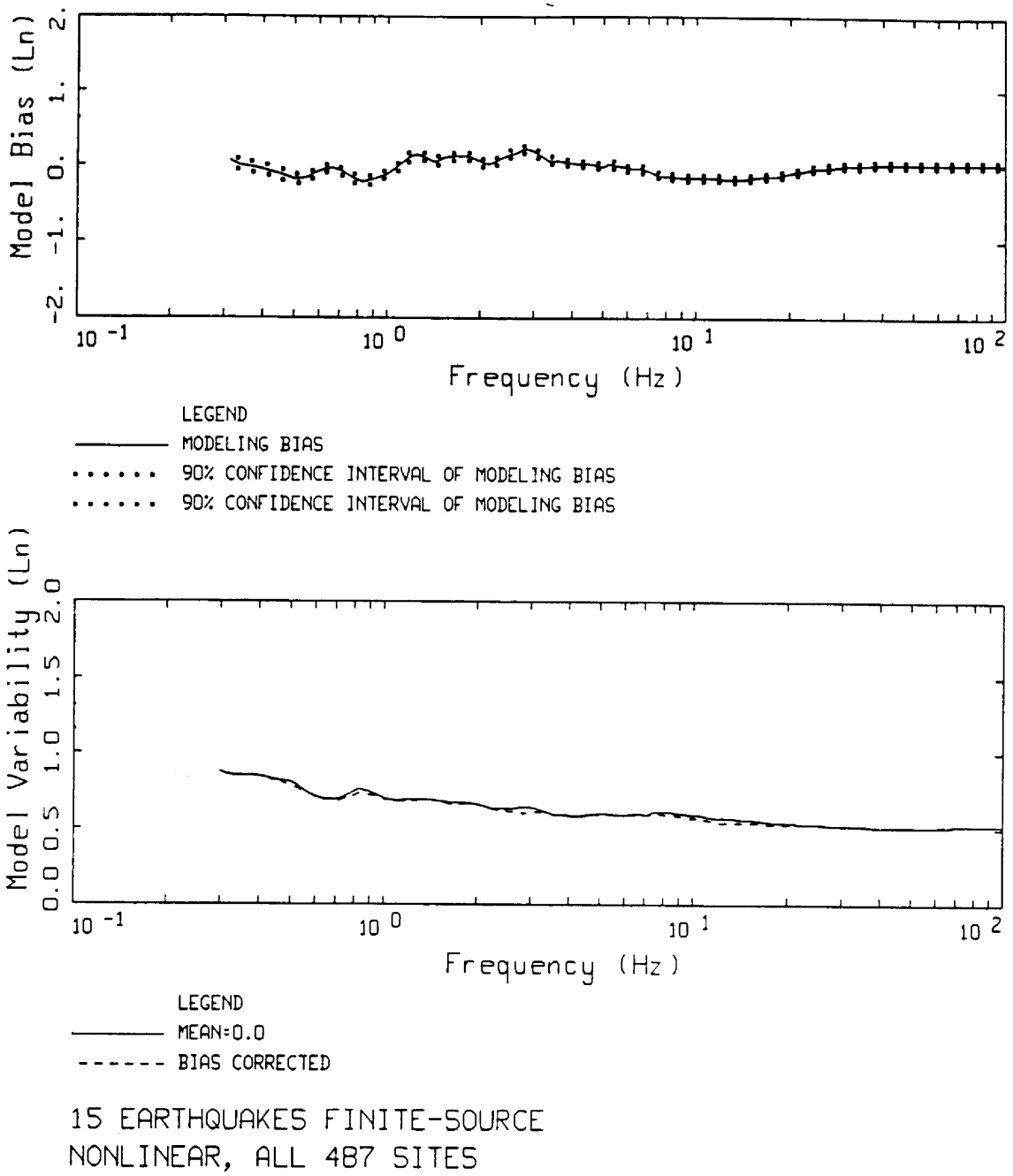

Figure A2. Model bias and variability estimates for all earthquakes computed over all 487 sites for the finite-source model.

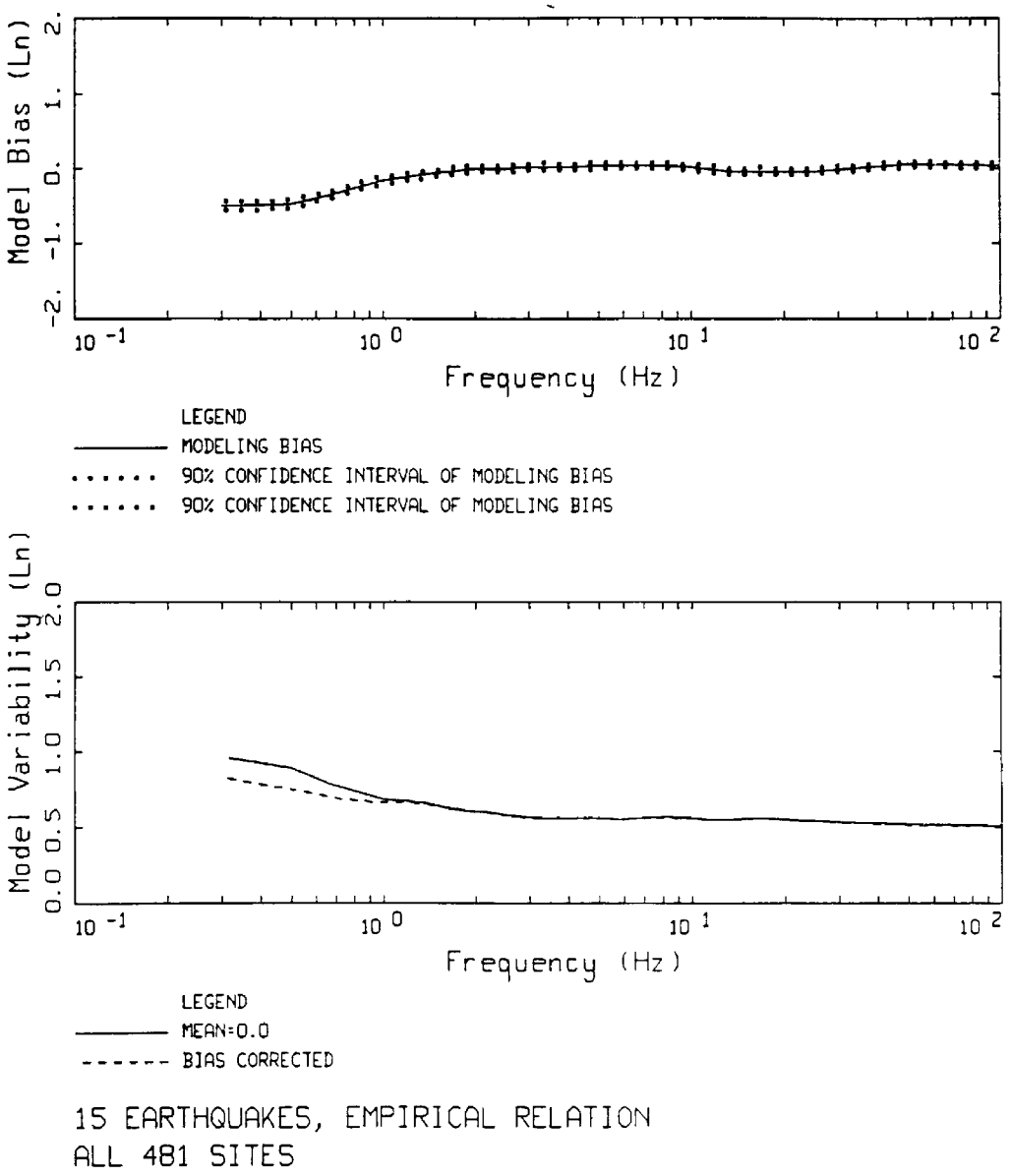

Figure A3. Model bias and variability estimates for all earthquakes computed over all 481 sites for the empirical model.

APPENDIX A

Development of Site Specific Soil Motions

The conventional approach to estimating the effects of site-specific site conditions on strong ground motions involves development of a set (1, 2, or 3 component) of time histories compatible with the specified outcrop response spectra to serve as control (or input) motions. The control motions are then used to drive a nonlinear computational formulation to transmit the motions through the profile. Simplified analyses generally assume vertically propagating shear-waves for horizontal components and vertically propagating compression-waves for vertical motions. These are termed one-dimensional site response analyses.

Equivalent-Linear Computational Scheme

The computational scheme which has been most widely employed to evaluate one-dimensional site response assumes vertically-propagating plane shear-waves. Departures of soil response from a linear constitutive relation are treated in an approximate manner through the use of the equivalent-linear approach.

The equivalent-linear approach, in its present form, was introduced by Seed and Idriss (1970). This scheme is a particular application of the general equivalent-linear theory developed by Iwan (1967). Basically, the approach is to approximate a second order nonlinear equation, over a limited range of its variables, by a linear equation. Formally this is done in such a way that the average of the difference between the two systems is minimized. This was done in an ad-hoc manner for ground response modeling by defining an effective strain which is assumed to exist for the duration of the excitation. This value is usually taken as 65% of the peak time-domain strain calculated at the midpoint of each layer, using a linear analysis. Modulus reduction and hysteretic damping curves are then used to define new parameters for each layer based on the effective strain computations. The linear response calculation is repeated, new effective strains evaluated, and iterations performed until the changes in parameters are below some tolerance level. Generally a few iterations are sufficient to achieve a strain-compatible linear solution.

This stepwise analysis procedure was formalized into a one-dimensional, vertically propagating shear-wave code called SHAKE (Schnabel et al., 1972). Subsequently, this code has easily become the most widely used analysis package for one-dimensional site response calculations.

The advantages of the equivalent-linear approach are that parameterization of complex nonlinear soil models is avoided and the mathematical simplicity of a linear analysis is preserved. A truly nonlinear approach requires the specification of the shapes of hysteresis curves and their cyclic dependencies through an increased number of material parameters. In the equivalent-linear methodology the soil data are utilized directly and, because at each iteration the problem is linear and the material properties are frequency independent, the damping is rate independent and hysteresis loops close.

Careful validation exercises between equivalent-linear and fully nonlinear formulations using recorded motions from 0.05 to 0.50g showed little difference in results (EPRI, 1993). Both formulations compared very favorably to recorded motions suggesting both the adequacy of the vertically propagating shear-wave model and the approximate equivalent-linear formulation. While the assumptions of vertically propagating shear-waves and equivalent-linear soil response certainly represent approximations to actual conditions, their combination has achieved demonstrated success in modeling observations of site effects and represent a stable, mature, and reliable means of estimating the effects of site conditions on strong ground motions (Schnabel et al., 1972; Silva et al., 1988; Schneider et al., 1993; EPRI, 1993).

To accommodate both uncertainty and randomness in dynamic material properties, analyses are typically done for the best estimate shear-wave velocity profile as well as upper- and lower-range profiles. The upper- and lower-ranges are usually specified as twice and one-half the best

estimate shear-wave moduli. Depending upon the nature of the structure, the final design spectrum is then based upon an envelope or average of the three spectra.

For vertical motions, the SHAKE code is also used with compression-wave velocities and damping substituted for the shear-wave values. To accommodate possible nonlinear response on the vertical component, since modulus reduction and hysteretic damping curves are not generally available for the constrained modulus, the low-strain Poisson's ratio is usually fixed and strain compatible compression-wave velocities calculated using the strain compatible shear moduli from the horizontal component analyses combined with the low-strain Poisson's ratios. In a similar manner, strain compatible compression-wave damping values are estimated by combining the strain compatible shear-wave damping values with the low-strain damping in bulk or pure volume change. This process assumes the loss in bulk (volume change) is constant or strain independent. Alternatively, zero loss in bulk is assumed and the equation relating shear- and compression-wave damping (η_S and η_P) and velocities (V_S and V_P)

$$\eta_P \approx \frac{4}{3}\frac{V_S}{V_P}\eta_S, \qquad \text{(B-1)}$$

is used.

RVT Based Computational Scheme

The computational scheme employed to compute the site response for this project uses an alternative approach employing random vibration theory (RVT). In this approach the control motion power spectrum is propagated through the one-dimensional soil profile using the plane-wave propagators of Silva (1976). In this formulation only SH waves are considered. Arbitrary angles of incidence may be specified but normal incidence is used throughout the present analyses.

In order to treat possible material nonlinearities, an RVT based equivalent-linear formulation is employed. Random process theory is used to predict peak time domain values of shear-strain based upon the shear-strain power spectrum. In this sense the procedure is analogous to the program SHAKE except that peak shear-strains in SHAKE are measured in the time domain. The purely frequency domain approach obviates a time domain control motion and, perhaps just as significant, eliminates the need for a suite of analyses based on different input motions. This arises because each time domain analysis may be viewed as one realization of a random process. Different control motion time histories reflecting different time domain characteristics but with nearly identical response spectra can result in different nonlinear and equivalent-linear response.

In this case, several realizations of the random process must be sampled to have a statistically stable estimate of site response. The realizations are usually performed by employing different control motions with approximately the same level of peak accelerations and response spectra.

In the case of the frequency domain approach, the estimates of peak shear-strain as well as oscillator response are, as a result of the random process theory, fundamentally probabilistic in nature. For fixed material properties, stable estimates of site response can then be obtained with a single run.

In the context of the RVT equivalent-linear approach, a more robust method of incorporating uncertainty and randomness of dynamic material properties into the computed response has been developed. Because analyses with multiple time histories are not required, parametric

variability can be accurately assessed through a Monte Carlo approach by randomly varying dynamic material properties. This results in median as well as other fractile levels (e.g. 16^{th}, mean, 84^{th}) of smooth response spectra at the surface of the site. The availability of fractile levels reflecting randomness and uncertainty in dynamic material properties then permits a more rational basis for selecting levels of risk.

In order to randomly vary the shear-wave velocity profile, a profile randomization scheme has been developed which varies both layer velocity and thickness. The randomization is based on a correlation model developed from an analysis of variance on about 500 measured shear-wave velocity profiles (EPRI, 1993; Silva et al., 1997). Profile depth (depth to competent material) is also varied on a site specific basis using a uniform distribution. The depth range is generally selected to reflect expected variability over the structural foundation as well as uncertainty in the estimation of depth to competent material.

To model parametric variability for compression-waves, the base-case Poisson's ratio is generally fixed. Suites of compatible random compression- and shear-wave velocities are then generated based on the random shear-wave velocities profiles.

To accommodate variability in modulus reduction and hysteretic damping curves on a generic basis, the curves are independently randomized about the base case values. A log normal distribution is assumed with a σ_{ln} of 0.35 at a cyclic shear strain of 3×10^{-2}%. These values are based on an analysis of variance on a suite of laboratory test results. An upper and lower bound truncation of 2σ is used to prevent modulus reduction or damping models that are not physically possible. The random curves are generated by sampling the transformed normal distribution with a σ_{ln} of 0.35, computing the change in normalized modulus reduction or percent damping at 3×10^{-2}% shear strain, and applying this factor at all strains. The random perturbation factor is reduced or tapered near the ends of the strain range to preserve the general shape of the median curves (Silva, 1992).

To model vertical motions, incident inclined compression- and shear (SV)-waves are assumed. Raytracing is done from the source location to the site to obtain appropriate angles of incidence. In the P-SV site response analyses, linear response is assumed in both compression and shear with the low-strain shear-wave damping used for the compression-wave damping (Johnson and Silva, 1981). The vertical and horizontal motions are treated independently in separate analyses. Validation exercises with a fully 3-D soil model using recorded motions up to 0.50%g showed these approximations to be validate (EPRI, 1993).

In addition, the site response model for the vertical motions has been validated at over 100 rock and soil sites for three large earthquakes: 1989 **M** 6.9 Loma Prieta, 1992 **M** 7.2 Landers, and the 1994 Northridge earthquakes. In general, the model performs well and captures the site and distance dependency of vertical motions over the frequency range of about 0.3 to 50.0 Hz and the fault distance range of about 1 to 100 km.

APPENDIX A

REFERENCES

Electric Power Research Institute (1993). "Guidelines for determining design basis ground motions." Palo Alto, Calif: Electric Power Research Institute, vol. 1-5, EPRI TR-102293.
vol. 1: Methodology and guidelines for estimating earthquake ground motion in eastern North America.
vol. 2: Appendices for ground motion estimation.
vol. 3: Appendices for field investigations.
vol. 4: Appendices for laboratory investigations.
vol. 5: Quantification of seismic source effects.

Iwan, W.D. (1967). "On a class of models for the yielding behavior of continuous and composite systems." *J. Appl. Mech.,* 34, 612-617.

Johnson, L.R. and W.J. Silva (1981). "The effects of unconsolidated sediments upon the ground motion during local earthquakes." *Bull. Seism. Soc. Am.*, 71, 127-142.

Schnabel, P.B., J. Lysmer, and H.B. Seed (1972). *SHAKE: a Computer Program for Earthquake Response Analysis of Horizontally Layered Sites.* Earthq. Engin. Res. Center, Univ. of Calif. at Berkeley, EERC 72-12.

Schneider, J.F., W.J. Silva, and C.L. Stark (1993). Ground motion model for the 1989 **M** 6.9 Loma Prieta earthquake including effects of source, path and site. *Earthquake Spectra,* 9(2), 251-287.

Seed, H.B. and I.M. Idriss (1970). "*Soil Moduli and Damping Factors for Dynamic Response Analyses,"* Earthq. Eng. Res. Center, Univ. of Calif. at Berkeley, Report No. UCB/EERC-70/10.

Silva, W.J., N. Abrahamson, G. Toro, and C. Costantino (1997). "Description and validation of the stochastic ground motion model." Submitted to Brookhaven National Laboratory, Associated Universities, Inc. Upton, New York.

Silva, W.J. (1992). "Factors controlling strong ground motions and their associated uncertainties." *Dynamic Analysis and Design Considerations for High Level Nuclear Waste Repositories, ASCE* 132-161.

Silva, W. J., T. Turcotte, and Y. Moriwaki, (1988). "Soil Response to Earthquake Ground Motion," Electric Power Research Institute, Walnut Creek, California, Report No. NP-5747.

Silva, W.J. (1976). "Body Waves in a Layered Anelastic soilid." *Bull. Seis. Soc. Am.*, vol. 66(5), 1539-1554.

APPENDIX A